

SURFACE-ENHANCED RAMAN SCATTERING TECHNIQUE FOR POLYCYCLIC AROMATIC
HYDROCARBONS DETECTION USING THIOL-FUNCTIONALIZED SILVER NANOPARTICLE
FILMS



A Thesis Submitted in Partial Fulfillment of the Requirements
for the Degree of Master of Science in Petrochemistry and Polymer Science
Field of Study of Petrochemistry and Polymer Science
Faculty of Science
Chulalongkorn University
Academic Year 2018
Copyright of Chulalongkorn University

เทคนิคเซอร์เฟซ-เอ็นฮานซ์รามานสแกตเทอริงสำหรับการตรวจวัดพอลิไซคลิกแอโรแมติกไฮโดรคาร์บอนโดยใช้ฟิล์มอนุภาคระดับนาโนเมตรของเงินที่ปรับปรุงด้วยสารประกอบไทออล



วิทยานิพนธ์นี้เป็นส่วนหนึ่งของการศึกษาตามหลักสูตรปริญญาวิทยาศาสตรมหาบัณฑิต สาขาวิชาปิโตรเคมีและวิทยาศาสตร์พอลิเมอร์ สาขาวิชาปิโตรเคมีและวิทยาศาสตร์พอลิเมอร์ คณะวิทยาศาสตร์ จุฬาลงกรณ์มหาวิทยาลัย
ปีการศึกษา 2561
ลิขสิทธิ์ของจุฬาลงกรณ์มหาวิทยาลัย

Thesis Title SURFACE-ENHANCED RAMAN SCATTERING TECHNIQUE FOR
POLYCYCLIC AROMATIC HYDROCARBONS DETECTION USING
THIOL-FUNCTIONALIZED SILVER NANOPARTICLE FILMS

By Miss Sathita Taksadej

Field of Study Petrochemistry and Polymer Science

Thesis Advisor Assistant Professor Prompong Pienpinijtham, Ph.D.

Co Advisor Assistant Professor Kanet Wongravee, Ph.D.

Accepted by the Faculty of Science, Chulalongkorn University in Partial Fulfillment of
the Requirement for the Master of Science

..... Dean of the Faculty of Science
(Associate Professor Polkit Sangvanich, Ph.D.)

THESIS COMMITTEE

..... Chairman
(Assistant Professor Warinthorn Chavasiri, Ph.D.)

..... Advisor
(Assistant Professor Prompong Pienpinijtham, Ph.D.)

..... Co-Advisor
(Assistant Professor Kanet Wongravee, Ph.D.)

..... Examiner
(Prasit Pattananuwat, Ph.D.)

..... External Examiner
(Nattawadee Wisitruangsakul, Ph.D.)

สาธิตา ทักษเดช : เทคนิคเซอร์เฟซ-เอ็นฮานซ์รามานสแกตเทอริงสำหรับการตรวจวัดพอลิไซคลิกแอโรแมติกไฮโดรคาร์บอนโดยใช้ฟิล์มอนุภาคระดับนาโนเมตรของเงินที่ปรับปรุงด้วยสารประกอบไทออล. (SURFACE-ENHANCED RAMAN SCATTERING TECHNIQUE FOR POLYCYCLIC AROMATIC HYDROCARBONS DETECTION USING THIOL-FUNCTIONALIZED SILVER NANOPARTICLE FILMS) อ.ที่ปรึกษาหลัก : ผศ. ดร.พร้อมพงศ์ เพียรพิณิจธรรม, อ.ที่ปรึกษาร่วม : ผศ. ดร.คณศ วังษ์ระวี

การตรวจวัดสารประกอบพอลิไซคลิกแอโรแมติกไฮโดรคาร์บอน (พีเอเอช) ถูกพัฒนาโดยมีพื้นฐานจากเทคนิคเซอร์เฟซ-เอ็นฮานซ์รามานสแกตเทอริง (SERS) ซึ่งใช้ฟิล์มอนุภาคระดับนาโนเมตรของเงินเป็นซับสเตรต ฟิล์มที่ใช้ถูกขึ้นรูปด้วยวิธีแลงเมียร์-บลอดเจตต์ และปรับปรุงพื้นผิวด้วยสารประกอบไทออลหลายชนิด ทั้งแอโรแมติก และอะลิฟาติกไทออล ได้แก่ แนฟทาลีนไทออล ฟีนิลอีเทนไทออล เพนเทนไทออล ออกเทนไทออล และโดเดเคนไทออล เพื่อสร้างชั้นที่มีสมบัติไม่ชอบน้ำให้พีเอเอชสามารถติดบนพื้นผิวและอยู่ในบริเวณฮอตสปอตได้ จากผลการทดลองสามารถบ่งชี้ได้ว่า พีเอเอช 9 ชนิดที่มีโครงสร้างต่างกัน ได้แก่ แอนทราซีน ไครซีน แนฟทาซีน แนฟทาลีน ฟีนนทรีน เพนทาซีน เพอร์ลิซิน ไพรีน และไทราฟีนีลีน สามารถติดอยู่บนฟิล์มอนุภาคระดับนาโนเมตรที่ปรับปรุงพื้นผิวด้วยสารประกอบไทออลได้ จากการที่รามานสเปกตรัมแสดงรูปแบบที่เป็นลักษณะเฉพาะของพีเอเอชแต่ละชนิด วิธีการทางเคโมเมทริกซ์ ได้แก่ เทคนิคการวิเคราะห์องค์ประกอบหลัก เทคนิคการแยกกลุ่ม เทคนิคการถดถอยกำลังสองน้อยที่สุดบางส่วน และเทคนิคการตรวจสอบไขว้แบบเอาออกทีละหนึ่ง ถูกนำมาใช้ในการวิเคราะห์ผลทั้งเชิงคุณภาพ และ เชิงปริมาณ สเปกตรัมที่ได้จากการตรวจวัดพีเอเอชชนิดเดียว (ที่ความเข้มข้นในช่วง 10^{-4} – 10^{-7} โมลาร์) ให้ผลการวิเคราะห์ที่มีประสิทธิภาพด้วยค่า R^2 มากกว่า 0.9800 และ Q^2 (R^2 ของการตรวจสอบแบบไขว้) มากกว่า 0.9300 ของผสมของพีเอเอช 2 ชนิดสามารถถูกวิเคราะห์ได้โดยให้ค่า R^2 มากกว่า 0.9700 และ Q^2 มากกว่า 0.8900 นอกจากนี้ ความเข้มข้นรวมของของผสมของพีเอเอช 9 ชนิดสามารถถูกวิเคราะห์ได้โดยให้ค่า $R^2 = 0.9700$ และ $Q^2 = 0.9196$ วิธีการนี้สามารถนำไปใช้ในการตรวจวัดพีเอเอชในตัวอย่างจริง เช่น ตรวจวัดพีเอเอชในน้ำได้ รวมถึงเทคนิคนี้สามารถให้ผลการทดลองที่มีประสิทธิภาพสูง โดยมีข้อดีคือ มีขั้นตอนการตรวจวัดที่รวดเร็ว ไม่ซับซ้อน และไม่มีการเตรียมสารตัวอย่างที่ยุ่งยากก่อนทำการตรวจวัด

สาขาวิชา	ปีเตอร์เคมีและวิทยาศาสตร์พอลิเมอร์	ลายมือชื่อนิสิต
ปีการศึกษา	2561	ลายมือชื่อ อ.ที่ปรึกษาหลัก
		ลายมือชื่อ อ.ที่ปรึกษาร่วม

5972118523 : MAJOR PETROCHEMISTRY AND POLYMER SCIENCE

KEYWORD:

Sathita Taksadej : SURFACE-ENHANCED RAMAN SCATTERING TECHNIQUE FOR POLYCYCLIC AROMATIC HYDROCARBONS DETECTION USING THIOL-FUNCTIONALIZED SILVER NANOPARTICLE FILMS. Advisor: Asst. Prof. Prompong Pienpinijtham, Ph.D.,Asst. Prof. Kanet Wongravee, Ph.D.

The detection of polycyclic aromatic hydrocarbons (PAHs) is developed based on surface-enhanced Raman scattering (SERS) using silver nanoparticle films as SERS substrates. The films are fabricated by a Langmuir Blodgett (LB) method and the surface of AgNP films are functionalized with various types of aromatic and aliphatic thiols, *i.e.*, naphthalenethiol, phenylethanethiol, pentanethiol, octanethiol, and dodecanethiol, to create a hydrophobic layer for PAHs to attach on and stay in hot spot. The results indicate that nine kinds of PAHs with different structures, *i.e.*, anthracene, chrysene, naphthacene, naphthalene, phenanthrene, pentacene, perylene, pyrene, and triphenylene, can attach on the surfaces of thiol-modified AgNP films as SERS spectra show characteristic patterns for each PAH. Chemometrics methods, *i.e.*, principle component analysis (PCA), cluster separation, partial least square (PLS) regression, and leave-one-out cross validation (LOOCV), are employed for qualitative and quantitative analysis. They show an effective analysis of pure PAH (at the concentration ranging from 10^{-4} – 10^{-7} M) results with the R^2 more than 0.9800 and Q^2 (R^2 of cross-validation model) more than 0.9300. The mixture of two PAHs can be determined with the R^2 more than 0.9700 and Q^2 more than 0.8900. Moreover, the total concentration of PAHs in the mixture of nine different PAHs can be analyzed with the $R^2 = 0.9700$ and $Q^2 = 0.9196$. This technique can be used to detect PAHs in real sample such as detect PAH in water matrix. SERS technique provides an advantage of sample analysis which does not require any complicated sample pretreatment, convenient and rapid *in situ* analysis with high sensitivity results.

Field of Study:	Petrochemistry and Polymer Science	Student's Signature
Academic Year:	2018	Advisor's Signature
		Co-advisor's Signature

ACKNOWLEDGEMENTS

First of all, I would like to express my gratitude to my thesis adviser Assistant Professor Dr. Prompong Pienpinijtham. This thesis cannot be successfully done without the help of my thesis adviser who generously provides me guidance, training, and encouragement during the experimental period and to help evaluating and finalizing this thesis, thank you for the patience to help and advice me. I would also like to express my gratitude to my co-adviser Assistant Professor Dr. Kanet Wongravee for encouraging me and for all advice and suggestion I need to complete my thesis. Also, I would like to thank my colleagues, Sensor Research Unit (SRU) member, for all the hospitality, help and support during my time doing this thesis.

I would like to sincerely thank Assistant Professor Dr. Warinthorn Chavasiri, Dr. Prasit Pattanauwat and Dr. Nattawadee Wisitruangsakul for being my thesis committee and giving all helpful suggestions.

Most of all, I would like to express my deepest gratitude to my parents and sisters for all their mental and physical support through all hard times with the considerate understanding and continuously cheering within these whole periods of times. Thank you for always be there for me and I am forever indebted to them for their incomparable love, help and support.

Finally, This thesis was supported by Faculty of science, Chulalongkorn University, thank you for providing all necessary facility for this project.

Sathita Taksadej

TABLE OF CONTENTS

	Page
ABSTRACT (THAI).....	iii
ABSTRACT (ENGLISH).....	iv
ACKNOWLEDGEMENTS.....	v
TABLE OF CONTENTS.....	vi
LIST OF TABLES.....	viii
LIST OF FIGURES.....	x
LIST OF ABBREVIATIONS.....	xiv
CHAPTER 1 INTRODUCTION.....	1
1.1 Problem and background.....	1
1.2 Objective.....	6
1.3 Scope.....	6
CHAPTER 2 THEORY.....	8
2.1 Polycyclic Aromatic Hydrocarbons (PAHs).....	8
2.2 Raman Spectroscopy.....	10
2.3 Surface-enhanced Raman Scattering (SERS).....	12
2.4 Langmuir-Blodgett (LB) Film.....	13
2.5 Data Analysis.....	15
CHAPTER 3 EXPERIMENTS.....	18
3.1 Chemicals.....	18
3.2 Synthesis of silver nanoparticles (AgNPs).....	18
3.3 Fabrication of AgNP film.....	19

3.4 SERS measurement	20
3.7 Data Analysis.....	22
CHAPTER 4 RESULTS AND DISCUSSION	24
4.1 Characterization of synthesized AgNPs colloid.....	24
4.2 Characterization of thiol-modified AgNP film.....	25
4.3 Detection of PAHs using thiol-modified AgNP films.....	28
4.4 Determination of PAH in two-PAHs mixture.....	53
4.5 Determination of the total concentration of PAHs in the mixture of nine different PAHs.....	62
CHAPTER 5 CONCLUSIONS.....	64
5.1 Conclusions.....	64
5.2 Suggestions.....	65
REFERENCES	66
VITA.....	75

LIST OF TABLES

	Page
Table 1.1 Conventional methods for PAHs detection.....	3
Table 1.2 SERS substrate for PAHs detection	5
Table 1.3 Thiol compounds used to modify the surface of AgNPs	7
Table 2.1 Names of PAHs with their molecular structures and molecular weights	9
Table 3.1 PAH concentrations in the mixtures of two different PAHs	21
Table 3.2 PAH concentrations in the mixture of 9 different PAHs	22
Table 4.1 Band assignments of thiol-modified AgNP films	27
Table 4.2 Band assignments of thiol-modified AgNP films with anthracene	30
Table 4.3 Band assignments of thiol-modified AgNP films with chrysene	31
Table 4.4 Band assignments of thiol-modified AgNP films with naphthacene.....	32
Table 4.5 Band assignments of thiol-modified AgNP films with naphthalene.....	33
Table 4.6 Band assignments of thiol-modified AgNP films with phenanthrene	34
Table 4.7 Band assignments of thiol-modified AgNP films with pentacene	35
Table 4.8 Band assignments of thiol-modified AgNP films with perylene.....	36
Table 4.9 Band assignments of thiol-modified AgNP films with pyrene	37

Table 4.10 Band assignments of thiol-modified AgNP films with triphenylene	38
Table 4.11 DBI value of different PAHs on different thiol-modified AgNP films	44
Table 4.12 R^2 of calibration curve and Q^2 of LOOCV for the determination of different PAHs.....	53
Table 4.13 R^2 of calibration curve and Q^2 of LOOCV of 2 PAHs mixture.....	61



LIST OF FIGURES

	Page
Figure 2.1 Energy level diagram involving Rayleigh scattering and Raman scattering..	11
Figure 2.2 Localized surface plasmon resonance (LSPR).	12
Figure 2.3 The arrangement of particles in the film at organic solvent-water interface.	14
Figure 4.1 (a) synthesized AgNPs colloid and (b) UV-visible spectrum of AgNPs colloid	24
Figure 4.2 (a) SEM image and (b) SERS spectra of thiol-modified AgNP film.....	25
Figure 4.3 SERS spectra of different PAHs at the concentration of 10^{-4} M on (a) PT-, (b) OT-, (c) DT-, (d) PhT-, and (e) NT- modified AgNP films.....	28
Figure 4.4 PCA plots of 9 PAHs on PT-modified AgNP film	39
Figure 4.5 PCA plots of 9 PAHs on PhT-modified AgNP film (a) full plot (b) expanded plot.....	40
Figure 4.6 PCA plots of 9 PAHs on OT-modified AgNP film	41
Figure 4.7 PCA plots of 9 PAHs on NT-modified AgNP film.....	41
Figure 4.8 PCA plots of 9 PAHs on PhT-modified AgNP film (a) full plot (b) expanded plot.....	42

Figure 4.9 SERS spectra of NT-modified AgNP films with (a) anthracene, (b) chrysene, (c) naphthacene, (d) naphthalene, and (e) triphenylene.....	45
Figure 4.10 SERS spectra of PT-modified AgNP films with (a) phenanthrene and (b) pyrene.....	46
Figure 4.11 SERS spectra of PhT-modified AgNP films with (a) pentacene and (b) perylene.	46
Figure 4.12 (i) PLS models and (ii) first loading plots of NT-modified AgNP films with (A) anthracene, (B) chrysene, and (C) naphthacene.....	48
Figure 4.13 (i) PLS models and (ii) first loading plots of NT-modified AgNP films with (A) naphthalene, and (B) triphenylene.....	49
Figure 4.14 (i) PLS models and (ii) first loading plots of PT-modified AgNP films with (A) phenanthrene and (B) pyrene.....	50
Figure 4.15 (i) PLS models and (ii) first loading plots of PhT-modified AgNP films with (A) pentacene and (B) perylene.....	51
Figure 4.16 SERS spectra of NT-modified AgNP films with (a) perylene in the presence of chrysene, (b) perylene in the presence of pyrene, (c) triphenylene in the presence of chrysene, (d) pyrene in the presence of pentacene, and (e) chrysene in the presence of naphthacene.....	54

Figure 4.17 PLS models for NT-modified AgNP films with (a) perylene in the presence of chrysene, (b) perylene in the presence of pyrene, (c) triphenylene in the presence of chrysene, (d) pyrene in the presence of pentacene, and (e) chrysene in the presence of naphthacene..... 55

Figure 4.18 First loading plots of NT-modified AgNP films with (a) perylene in the presence of chrysene, (b) perylene in the presence of pyrene, (c) triphenylene in the presence of chrysene, (d) pyrene in the presence of pentacene, and (e) chrysene in the presence of naphthacene. 56

Figure 4.19 SERS spectra of PhT-modified AgNP films with (a) perylene in the presence of chrysene, (b) perylene in the presence of pyrene, (c) triphenylene in the presence of chrysene, (d) pyrene in the presence of pentacene, and (e) chrysene in the presence of naphthacene. 57

Figure 4.20 PLS models for PhT-modified AgNP films with (a) perylene in the presence of chrysene, (b) perylene in the presence of pyrene, (c) triphenylene in the presence of chrysene, (d) pyrene in the presence of pentacene, and (e) chrysene in the presence of naphthacene..... 58

Figure 4.21 First loading plots of PhT-modified AgNP film with (a) perylene in the presence of chrysene, (b) perylene in the presence of pyrene, (c) triphenylene in the presence of chrysene, (d) pyrene in the presence of pentacene, and (e) chrysene in the presence of naphthacene. 59

Figure 4.22 SERS spectra of NT-modified AgNP film with the mixtures of 9 different PAHs.....	62
Figure 4.23 (a) PLS model and (b) first loading plot for NT-modified AgNP films with the mixtures of 9 different PAHs.....	63



LIST OF ABBREVIATIONS

AgNPs	Silver nanoparticles
AuNPs	Gold nanoparticles
MNPs	Metal nanoparticles
SERS	Surface-enhanced Raman scattering
PAHs	Polycyclic aromatic hydrocarbons
PT	Pentanethiol
DT	Dodecanethiol
OT	Octanethiol
NT	Naphthalenethiol
PhT	Phenylethanethiol
LB	Langmuir-Blodgett
PCA	Principal component analysis
PLS regression	Partial least square regression
PCs	Principal components
CSI	Cluster separation index
DBI	Davies Bouldin index
SNV	Standard normal variate
LOOCV	Leave-one-out cross validation

LSPR	Localized surface plasmon resonance
GC-MS	Gas chromatography with mass spectrometry
GC-FID	Gas chromatography with flame ionization detector
HPLC	High performance liquid chromatography
UV-DAD	UV-diode array detector
LC-UV	Liquid chromatography-UV
SEM	Scanning electron microscope
3-MPTMS	3-mercaptopropyl trimethoxysilane
APTMS	3-aminopropyl trimethoxysilane
CD-SH	per-6-deoxy-(6-thio)- β -cyclodextrin
CTAB	hexadecyl trimethyl ammonium bromide
rGO-AgNP	reduced graphene oxide-silver nanoparticle
LOD	Limit of detection

CHAPTER 1

INTRODUCTION

1.1 Problem and background

Polycyclic aromatic hydrocarbons (PAHs) are compounds built from two or more aromatic rings. They are neutral and non-polar. PAHs are formed by pyrolysis of organic matter at temperatures in the range of 500–900°C during combustion of fossil fuels, wood, waste incineration, and various industrial processes. The main sources of PAHs in environment are from human activities e.g. engine combustion, cigarette smoking and various food cooking operations such as frying, which produce PAH in frying oil after reused for several times. PAHs can also be produced when organic matters are transformed into fossil fuels.¹⁻² Burning solid fuel, such as coal in household, is the major PAHs emission in developing countries. PAHs usually stay in a complex form with heavy metals, which makes them difficult to be decomposed. PAHs are considered as carcinogenic, mutagenic, and teratogenic. PAHs can be exposed to human by various ways. For non-smokers, the exposure is majorly coming from food consumption and, for smokers, the exposure from smoking is more significant than from another pathway. Food can be contaminated from environmental sources, industrial food processing, and certain home cooking processes.³

There have been several methods to detect PAHs. For examples, Holsen, *et al.*⁴ used gas chromatography coupled with mass spectrometry (GC-MS) and gas chromatography with flame ionization detector (GC-FID) for the detection of PAHs

collected from airborne, coke ovens, and vehicles engines in Chicago metropolitan area. The collected samples were prepared within 24 hours after collected. The sample preparation method includes, extraction, volume reduction, sample clean up, and finally preconcentration before analyzed with GC-MS and GC-FID. According to the results, 20 types of PAHs were founded.

Budzinski, *et al.*⁵ used GC-MS to determine PAHs that were collected from Gironde estuary, France. The samples were extracted (with Soxhlet extractor) for 48 hours, reduced volume, desulfurized, and fractionated with microcolumn before analyzed with GC-MS. The detection range was 1000–2000 nanograms per gram of dry samples.

Friedlander, *et al.*⁶ used high performance liquid chromatography (HPLC) with fluorescence detector to measure PAHs from vehicle emission and surrounding aerosols from two traffic tunnels. The collected samples were extracted and fractionated before analyzed with HPLC. This method can be used to characterize PAHs with the size smaller than 1.0 μm .

Busetti, *et al.*⁷ detected 16 types of PAHs from wastewater plant in Venice, Italy by using HPLC with UV-diode array detector (UV-DAD). The sample preparation method includes HgCl_2 treatment, filtered, lyophilized, and extracted then analyzed with HPLC. The range of detection was 1.12–4.62 $\mu\text{g/L}$.

However, these methods need complicated sample pretreatment, long analysis time, expensive instruments, and operating skills. Moreover, these methods are difficult to perform outside laboratory. Table 1.1 shows the conventional techniques used to detect PAH with their detection limit.

Table 1.1 Conventional methods for PAHs detection

Year	Author	Technique	Detection Limit
1994	Venkataraman, <i>et al.</i>	HPLC with fluorescence detector	2–40 pg
1995	Khalili, <i>et al.</i>	GC-FID and GC-MS	0.124–1.42 ng
1997	Budzinski, <i>et al.</i>	GC-MS	1000–2000 ng/1g dry sample
2006	Buseti, <i>et al.</i>	HPLC with UV-DAD detector	1.12–4.62 µg/L

Surface-enhanced Raman scattering (SERS) technique is a sensitive spectroscopy technique widely used for the detection of trace substances by using metal nanoparticles (MNPs) as substrates to enhance the Raman signal. SERS technique can also be used to determine samples without any sample pretreatment. Because the surfaces of MNPs are polar, the non-polar molecules (such as PAHs) cannot attach on the surface of MNPs resulted in poor Raman signal. One important factor to obtain an efficient result from Raman signal is to increase the adsorption affinity between sample molecule and SERS substrate by modifying SERS substrates with chemicals that gives the appropriate property for substrate. Many previous works have reported the modification of SERS substrates for PAHs detection. For examples, Péron, *et al.*⁸ fabricate SERS substrate by functionalized quartz substrates through silanization reaction with 3-mercaptopropyl trimethoxysilane (MPTMS) or 3-aminopropyl trimethoxysilane (APTMS) then reacted with gold nanoparticles (AuNPs) colloidal suspension, subsequently. The obtained colloidal hydrophobic film

can be used to detect pyrene and naphthalene in artificial seawater with the limit of detection (LOD) at 7.8×10^{-11} M and 4.9×10^{-11} M, respectively.

Leyton, *et al.*⁹ fabricated SERS substrate by using silver nanoparticles (AgNPs), in suspension form or immobilized on glass, covered by self-assembled calix[4]arene molecules. The result shows that the interaction between calix[4]arene host molecule and PAH guest gives a selective result of four benzene rings PAHs, especially pyrene as the limit of detection can reach to 10^{-8} M range.

Xie, *et al.*¹⁰ fabricated SERS substrate by modifying AuNPs with per-6-deoxy-(6-thio)- β -cyclodextrin (CD-SH). Anthracene, pyrene, chrysene, triphenylene, and coronene can be detected, both in one component and mixture form.

Jiang, *et al.*¹¹ used hexadecyl trimethyl ammonium bromide (CTAB) micelle-assisted reduced graphene oxide-silver nanoparticle (rGO-AgNP) hybrids as SERS substrate to detect pyrene and perylene. The LOD can reach to 10^{-6} and 10^{-7} M, respectively.

Bao, *et al.*¹² used AuNPs embedded alginate gel as SERS substrate to detect pyrene, anthracene, fluorene and benzo(a)pyrene. Benzo(a)pyrene can be analyzed quantitatively with the LOD of 0.365 nM with the low-cost Raman spectrometer.

Schmidt, *et al.*¹³ used silver colloid encapsulated in sol-gel derived xerogel (fabricated by Lucht, *et al.*¹⁴ method) as SERS substrate to detect 6 PAHs; anthracene, benz(a)anthracene, fluoranthene, phenanthrene, and pyrene in seawater with LOD ranging from $\mu\text{g/L}$ to ng/L . Compared to conventional technique, SERS is an alternative technique for PAHs detection as it is a rapid, sensitive, non-destructive analysis technique, which doesn't require a complicated sample pretreatment.

Nowadays, Raman spectrometer is developed into portable instrument so many experiments can be done outside laboratory. Table 1.2 shows the choices of substrates used to detect PAHs and their sensitivity.

Table 1.2 SERS substrate for PAHs detection

Year	Author	Substrate	Sample
2004	Leyton, <i>et al.</i>	AgNPs on glass covered by adsorbed calix[4]arene molecules	- 8 PAHs - LOD: 10^{-8} M for pyrene
2004	Schmidt, <i>et al.</i>	Silver colloid encapsulated in sol-gel derived xerogel	- 6 PAHs - LOD: ranging from $\mu\text{g/L}$ to ng/L
2009	Péron, <i>et al.</i>	AuNPs on quartz (silanized with MPMS or APTMS)	- Naphthalene and pyrene - LOD: 7.8 and 4.9×10^{-11} M
2011	Xie, <i>et al.</i>	AuNPs modified with per-6-deoxy-(6-thio)- β -cyclodextrin (CD-SH)	- 5 PAHs: both individual and mixture
2012	Bao, <i>et al.</i>	AuNPs embedded alginate gel	- 4 PAHs - LOD: 0.365 nM for benzo(a)pyrene
2015	Jiang, <i>et al.</i>	CTAB micelle-assisted rGO-AgNP	- Pyrene and perylene - LOD: 10^{-6} and 10^{-7} M

In this study, we proposed surface-enhanced Raman scattering (SERS) technique as PAHs detection. Silver nanoparticles (AgNPs) were chosen to be a SERS substrate. However, PAHs cannot attach on AgNPs surface directly because they are nonpolar. Therefore, we functionalized the surface of AgNPs with thiol to create a nonpolar surface for PAHs to attach on a substrate. Also, we fabricated AgNPs substrate into films by using Langmuir-Blodgett (LB) method to make them convenient for using and storing.

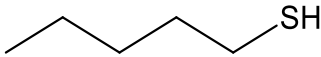
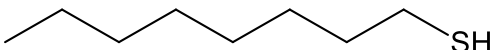
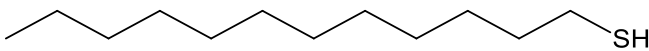
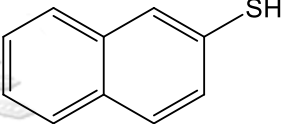
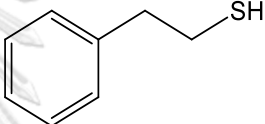
1.2 Objective

The objective of this work is to detect low concentration PAHs by surface-enhanced Raman scattering using thiol-modified AgNP film as SERS substrate.

1.3 Scope

- Fabricate AgNP film by LB method using 5 thiols, as shown in Table 1.3
- Detect PAHs with different concentrations using fabricated AgNP film as SERS substrate
- Analyze data by using chemometrics

Table 1.3 Thiol compounds used to modify the surface of AgNPs

Compound Name		Structure
Alkyl thiol	1-Pentanethiol	
	1-Octanethiol	
	1-Dodecanethiol	
Aromatic thiol	1-Naphthalenethiol	
	2-Phenylethanethiol	

CHAPTER 2

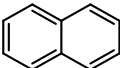
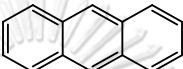
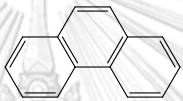
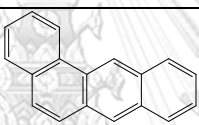
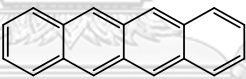
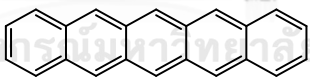
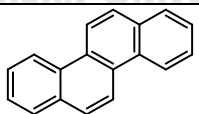
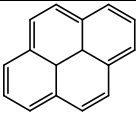
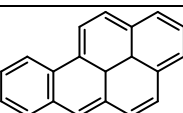
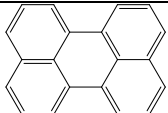
THEORY

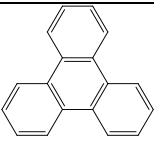

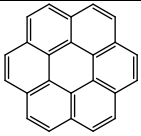
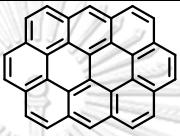
2.1 Polycyclic Aromatic Hydrocarbons (PAHs)

Polycyclic aromatic hydrocarbons (PAHs) are organic compounds consisting of multiple aromatic rings fused with one another (benzene is not considered to be PAHs). PAHs have boiling points between 150–325 °C and melting points between 101–438 °C. They also have no branch substitute for hydrogen from the structure. PAHs are non-polar, liposoluble, and neutral. They are found in fossil fuel, tar, and combustion of organic substances under oxygen insufficient condition. The more benzene ring in PAHs, the more difficult they can be degraded in environments.¹⁵⁻¹⁶ Conventional methods used to detect PAHs are GC-MS, GC-FID, LC-UV, and fluorescence spectroscopy. Each PAH has a unique UV absorption wavelength, even they are isomers. This property is very useful for PAHs identification.¹⁷ A previous study showed that a group of smokers had a trace of benzo[a]pyrene in a urine sample higher than the group of volunteers who had lung cancer without smoking as a result of PAHs from an incomplete burning of cigarettes. It indicates that PAH can be received and spread to other parts of human body.¹⁸ From the experiment to laboratory animal, PAHs spread to lung, liver, kidney, and gastrovascular system and it takes amount of time to eliminate PAHs from the body. This results in long term damage to body and may be developed into cancer.¹⁹ Also, enzyme in eukaryotic cells can change PAHs into epoxide form, that can attach to DNA, then change into

different types of metabolites, which some of them are carcinogen. The examples of PAHs with their structures and molecular weights are shown in Table 2.1.

Table 2.1 Names of PAHs with their molecular structures and molecular weights²⁰

Compound name	Structure	Molecular weight
Naphthalene		128.17
Anthracene		178.23
Phenanthrene		178.23
1,2-Benzanthracene		228.28
2,3-Benzanthracene (tetracene, naphthacene)		228.29
Benzo [b] naphthacene (pentacene)		278.35
Chrysene		228.29
Pyrene		202.26
Benzo [a] pyrene		252.31
Perylene		252.32

Triphenylene		228.29
Corannulene		250.29
Coronene		300.35
Ovalene		398.45

2.2 Raman Spectroscopy

Raman spectroscopy is an analytical technique used to identify substances through their vibrational spectrum pattern. While IR spectroscopy observes the functional groups of sample molecules by measuring the absorbance (or transmittance) of the light that passes through a sample, Raman spectroscopy observes the shift in wavelength of scattered light after interacting with the molecules and provides the information about sample identification and quantification. Raman bands are originated from changes in polarizability of molecules because of the molecular deformation in electric field. Each substance has its own spectral pattern (so-called “molecular fingerprint”), when the chemical bonds change their vibrational modes, the emission wavelength are also change compared to the applied incident light. From Figure 2.1, if the final vibrational energy state of molecules is higher than the initial (molecules gain energy and photons lose energy), the frequency of photons will be red-shifted (shifted to a lower frequency),

called Stokes shift. On the other hand, if the final state is lower than the initial (molecules lose energy and photons gain energy), the frequency of photon will be blue-shifted (shifted to a higher frequency), called anti-Stokes shift.²¹⁻²²

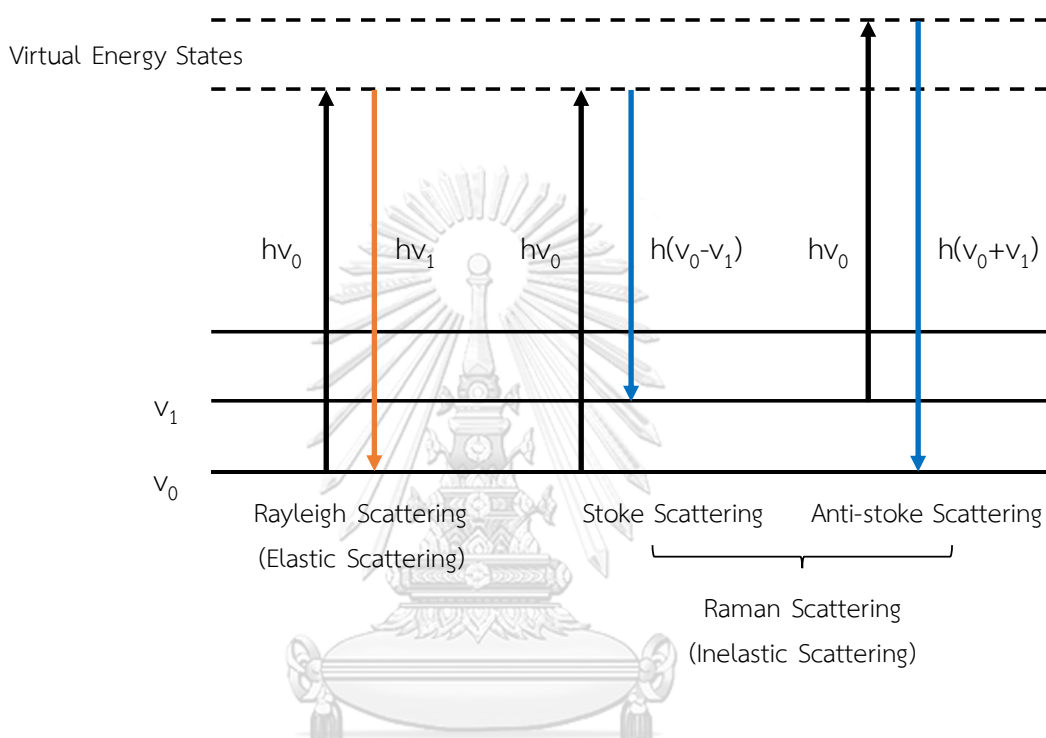


Figure 2.1 Energy level diagram involving Rayleigh scattering and Raman scattering.

The advantages of Raman spectroscopy over IR spectroscopy are (i) very weak Raman scattering efficiency of water and carbon dioxide (CO_2) molecules, which make them not be considered as interferences (ii) little or no sample pretreatment (iii) inexpensive sample holder/carrier. Raman spectroscopy can be used to determine solid, liquid, and gaseous samples. However, the scattering efficiency of molecules is normally low as more than 99% of scattered light are normally Rayleigh

scattering (elastic scattering). So, the detection of low concentrations and small amount of samples is hard to perform.²³⁻²⁴

2.3 Surface-enhanced Raman Scattering (SERS)

Surface-enhanced Raman scattering (SERS) is a technique which helps increase Raman signal intensity and widely used for trace substance analysis. By using metal nanoparticles (MNPs), such as silver nanoparticles (AgNPs) or gold nanoparticles (AuNPs), as a SERS substrate, the Raman signal intensities are greatly enhanced. The enhancement occurs through localized surface plasmon resonance (LSPR) phenomenon. Briefly, by applying the external light with the same frequency (or wavelength) as the plasmon (the electron clouds oscillating around metal surface), the plasmon resonates and induces electric field enhancement around the metal surface. (Figure 2.2).²⁵

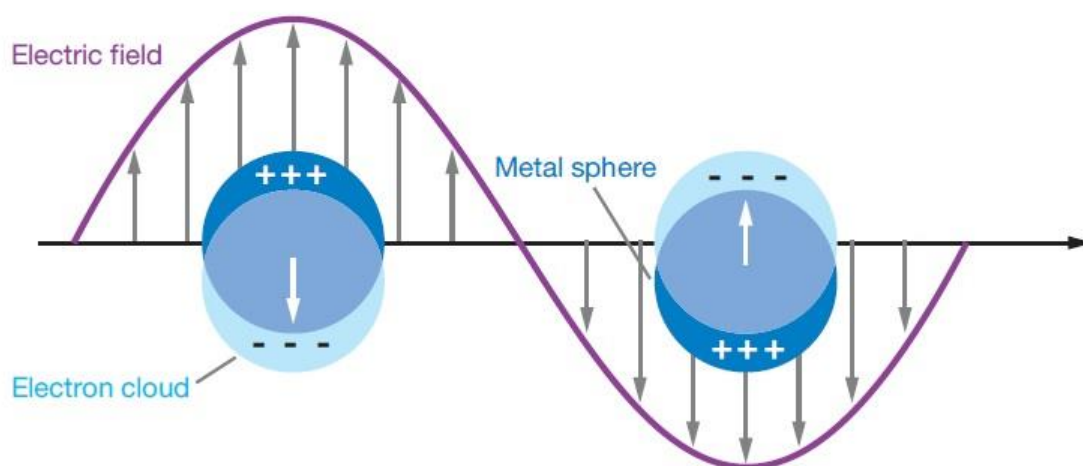


Figure 2.2 Localized surface plasmon resonance (LSPR).²⁶

The electric field enhancement around the metal surface make the adsorbed molecules on metal nanoparticles scatter light more effectively resulted in the increase of Raman signal intensity. This is known as an electromagnetic mechanism and the area where the electric field is more intense is called “hot spot”. Gold and silver are commonly used because the oscillation frequencies (or wavelengths) of plasmons on the surfaces are in the visible region, and they are quite stable in ambient conditions. Also, the charge that transfers between a substrate and a sample molecule can enhance the signal through a chemical mechanism.²⁶⁻²⁸ The sensitivity and selectivity of SERS technique can be improved even more by increasing the adsorption between sample molecules and SERS substrates. One choice is to functionalize the surface with the molecule that create suitable environment around metal surface. Metal nanoparticles are commonly used in a colloid form which is inconvenient to store and is not much stable compared to a solid form. Fabricating film as SERS substrates is another method to achieve a stable and convenient substrate for sample detection. In this work, we used AgNPs because they give the highest electric field enhancement in visible region and can be easily prepared using few chemicals and simple procedure.²⁹

2.4 Langmuir-Blodgett (LB) Film

Langmuir-Blodgett (LB) is one of the common methods for the preparation of thin films because it provides a homogeneous deposition over large areas. LB films are formed when metal nanoparticles in an aqueous phase were pushed up to the

organic solvent–water interface and interact with organic substances in an organic phase by injecting a low dielectric solvent into the aqueous phase. Nanoparticles move out from an aqueous phase because the polarity of water decrease. However, they cannot go across to an organic phase and are stuck as a film at the interface. After organic solvent dries out, the metal nanoparticles have organic substances depositing on their surface. LB method provides a control over the formation of molecules in monolayer that are difficult to successfully achieve from other methods. The applications of LB film are electronics, chemical sensors, and biosensors.³⁰⁻³¹

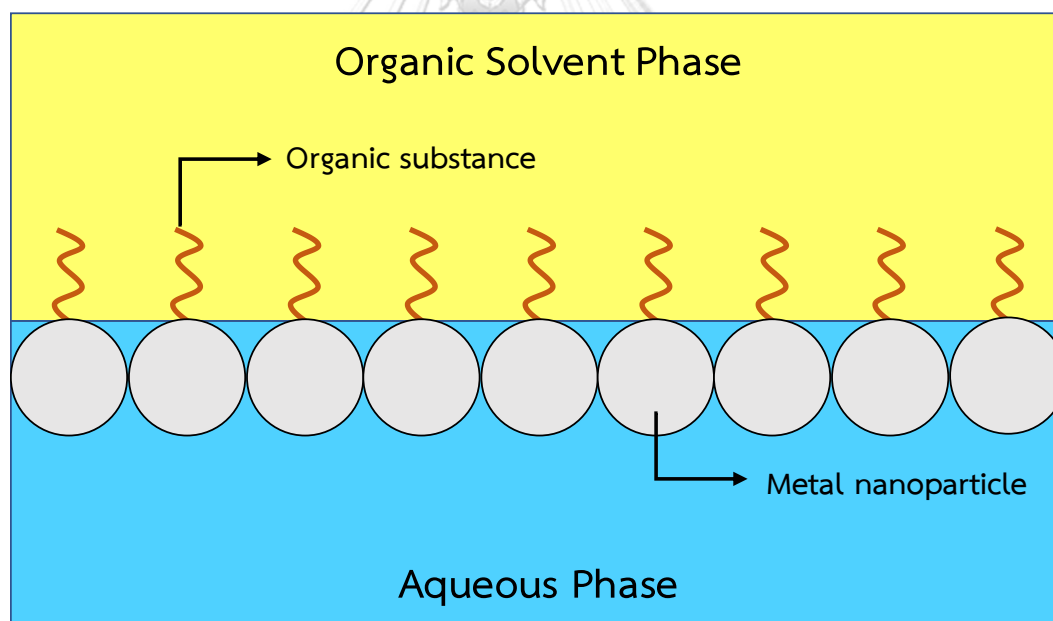
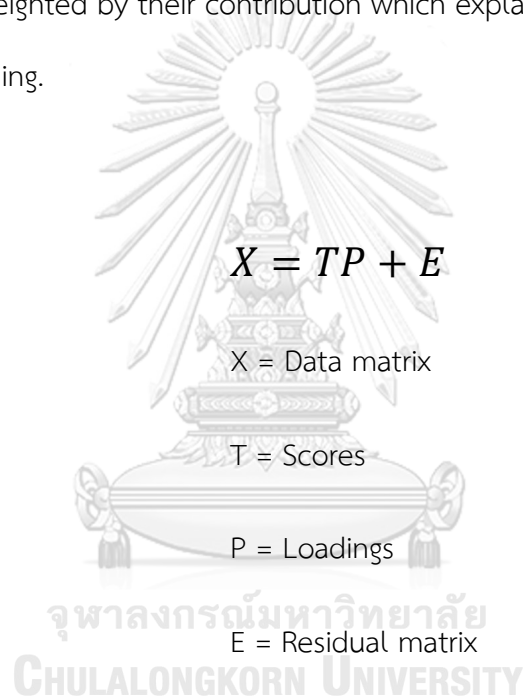


Figure 2.3 The arrangement of particles in the film at organic solvent-water interface.

2.5 Data Analysis

Principal component analysis (PCA) is one of the multivariate data analysis. It is a mathematical method that reducing large set of variables into small data set that still contains most information from the raw data. By following the Equation (1), the important information from the data is extracted and expressed as a set of new orthogonal variables called principal components (PCs). PCs are linear combinations of the variables weighted by their contribution which explain the variance in the form of scores and loading.



$$X = TP + E \quad (1)$$

X = Data matrix
 T = Scores
 P = Loadings
 E = Residual matrix

To classify the data into groups (or so-called clusters), cluster separation analysis is required. The data are separated according to their similarity and dissimilarity. The data with similar pattern are classified to be in the same group. After obtaining the data cluster, it is significant to consider how well these clusters separate from each other. If two clusters can be easily distinguished from one another, it means that there is a significant factor that influence the results. So, cluster separation index (CSI) is used to determine the distance between clusters.

There are many CSIs but, in this work, we use Davies Bouldin index (DBI). DBI is widely used to determine cluster separation, which the separations are considered from the inter-cluster distance of 2 clusters centroids (center of the cluster) with intra-distance, as shown in Equation (2). The lower value indicates the smaller overlapping between 2 clusters.³²⁻³⁵

$$DBI = \frac{1}{2} \left(\frac{d_2(A) + d_2(B)}{d(A,B)} \right) \quad (2)^{36}$$

$d(A, B)$ = inter-cluster distance

$d_2(A), d_2(B)$ = intra-cluster distance

Partial least square (PLS) regression is a supervised pattern recognition technique for creating predictive model from the latent structure of datasets. PLS regression can also be used to select a suitable variable for prediction. By considering the least square fit on the variables, the linear combination of the original variables is created.³⁷⁻³⁸ The PLS model is normally gives a fairly good results, because the model was created from the data itself. However, this does not confirm that the model can actually be used. The cross-validation method is proposed to test the ability of the prediction model created from PLS. The test set is created by using some samples from the raw data. The set is assumed to be an unknown sample which will be predicted by the model obtained from the remaining samples or so-called calibration set. In this work, leave-one-out cross-validation (LOOCV), which one sample is picked as a test set, is used as a cross-validation method. The efficiency of

the obtained PLS and cross-validation model is expressed in the form of R^2 and Q^2 value, by which Q^2 is the R^2 of the cross-validation model.³⁹⁻⁴¹



CHAPTER 3

EXPERIMENTS

3.1 Chemicals

Ethanol, hydrogen peroxide (H_2O_2), and sulfuric acid (H_2SO_4) were purchased from Merck. Octanethiol (OT), pentanethiol (PT), dodecanethiol (DT), naphthalenethiol (NT), phenylethanethiol (PhT), chrysene, and 3-mercaptopropyl trimethoxysilane (3-MPTMS), were purchased from Sigma-Aldrich Co., Ltd. Silver nitrate ($AgNO_3$), trisodium citrate dihydrate, hexane and naphthalene were purchased from Aencore Chemical Co., Ltd., Carlo Erba Reagents S.A.S., Fischer Scientific, and JT Baker, respectively. Perylene, pyrene, triphenylene were purchased from Dr.Ehrenstorfer GmbH. All chemicals were used as received without any further purification. DI water was employed as a solvent for preparing all aqueous solutions.

3.2 Synthesis of silver nanoparticles (AgNPs)

Silver nanoparticle colloid was synthesized using previously proposed synthesis method.²⁹ Briefly, ninety milligrams of silver nitrate was dissolved in 500 mL water, and then heated until boiling. A solution of 1% trisodium citrate (10 mL) was suddenly added into a boiling silver nitrate solution. The colorless mixture turned yellow immediately, which indicates the formation of small silver nanoparticles. The mixture was stirred vigorously and kept boiling for 1 hour. Finally, the mixture color changed from yellow to yellow–grey. After the mixture was cooled down to room

temperature, the volume of the mixture was adjusted back to 500 mL using DI water. The synthesized silver nanoparticle colloid was characterized by UV-visible spectrometer and scanning electron microscope.

3.3 Fabrication of AgNP film

The glass slide was cut into the size of $0.5 \times 0.5 \text{ cm}^2$ using a diamond tipped glass cutter. The cut glass slides were immersed in a piranha solution ($\text{H}_2\text{SO}_4:\text{H}_2\text{O}_2 = 7:3$) and boiled for 30 minutes. After that, they were rinsed with DI water and ethanol, then soaked into a 2% of 3-mercaptopropyltrimethoxysilane (3-MPTMS) in ethanol solution overnight. Finally, they were rinsed off by ethanol to remove excess 3-MPTMS.

To fabricate AgNP film, the Langmuir-Blodgett method was used.³⁰ Briefly, 0.5 μL of alkyl thiol was dissolved into 10 mL of hexane. Then, the hexane solution was gently poured onto 20 mL of silver nanoparticle colloid to develop a hexane/water interface. After that, 12 mL of ethanol was slowly injected into the water phase. The shiny silver mirror film can be observed at the hexane/water interface. Hexane was then slowly evaporated at ambient conditions, which left the AgNP film on the surface of water phase. The AgNP film was transferred to the glass slide by dipping the modified glass slide into the water phase, and then lifted vertically to cover the glass slide with AgNP film. AgNPs bind to the glass slide by thiol groups of 3-MPTMS on the surface. The dried film on glass slide was soaked in hexane for 15 min in order to remove excess chemicals. Finally, the film was dried at room temperature and kept in desiccators for further use.

3.4 SERS measurement

The prepared AgNP films were separately immersed into different ethanoic solutions of PAHs with desired concentrations (1.0×10^{-4} , 5.0×10^{-5} , 1.0×10^{-5} , 5.0×10^{-6} , 1.0×10^{-6} , 5.0×10^{-7} , and 1.0×10^{-7} M) for 15 minutes then rinsed gently with ethanol. SERS spectra of these films were collected using DXR Raman microscope (Thermo Scientific) with a 532-nm excitation laser. Laser power was at 10 mW and laser spot was 50 μ m slit. All spectra were collected using 16 accumulations with the accumulation time of 2 seconds. Each sample was measured at 5 different areas on the film. Any spectral correction was not applied to all presented SERS spectra.

Mixtures of 2 different of PAHs were prepared by varying the concentration of one kind of analyzed PAH (1×10^{-4} , 1×10^{-5} , 5×10^{-6} , 1×10^{-6} , and 5×10^{-7} M) mixed with another interfering PAH with the concentrations shown in Table 3.1. Then, the mixtures were measured using PhT- and NT-modified AgNP films.

Table 3.1 PAH concentrations in the mixtures of two different PAHs

Mixture	Analyzed PAH	Interfering PAH
1	Perylene	Chrysene (1×10^{-6} M)
2	Perylene	Pyrene (1×10^{-5} M)
3	Triphenylene	Chrysene (1×10^{-6} M)
4	Pyrene	Pentacene (1×10^{-6} M)
5	Chrysene	Naphthacene (1×10^{-5} M)

Five mixtures of 9 different PAHs were prepared by mixing PAHs with the concentrations shown in Table 3.2, then SERS spectra of mixture were measured using NT-modified AgNP film.

Table 3.2 PAH concentrations in the mixture of 9 different PAHs

	Mixture				
	1	2	3	4	5
Anthracene	10^{-5} M	5×10^{-6} M	10^{-6} M	5×10^{-7} M	10^{-7} M
Chrysene	5×10^{-6} M	10^{-5} M	10^{-6} M	5×10^{-7} M	10^{-7} M
Naphthacene	10^{-5} M	5×10^{-6} M	10^{-6} M	5×10^{-7} M	10^{-7} M
Naphthalene	10^{-5} M	5×10^{-6} M	10^{-6} M	5×10^{-7} M	10^{-7} M
Phenanthrene	10^{-5} M	5×10^{-6} M	10^{-6} M	5×10^{-7} M	10^{-7} M
Pentacene	10^{-5} M	5×10^{-6} M	10^{-6} M	5×10^{-7} M	10^{-7} M
Perylene	10^{-5} M	10^{-6} M	5×10^{-6} M	5×10^{-7} M	10^{-7} M
Pyrene	10^{-5} M	5×10^{-6} M	10^{-6} M	5×10^{-7} M	10^{-7} M
Triphenylene	10^{-5} M	5×10^{-6} M	10^{-6} M	5×10^{-7} M	10^{-7} M

3.7 Data Analysis

Chemometric was used to analyze the SERS spectra data using MATLAB (Mathwork, Inc. Version R2018a). Principal component analysis (PCA), cluster separation, partial least square (PLS), and leave-one-out cross validation (LOOCV) were used for qualitative and quantitative analyses.

First, the raw spectra were preprocessed by a standard normal variate (SNV) method. For qualitative analysis, the preprocessed data were undergone PCA procedure with number of components of 3. Then the obtained data were processed using cluster separation technique to achieve DBI. For quantitative analysis, the preprocessed data were undergone by PLS procedure and LOOCV to achieve the calibration curve and the cross-validation model of the obtained calibration curve.



CHAPTER 4

RESULTS AND DISCUSSION

4.1 Characterization of synthesized AgNPs colloid

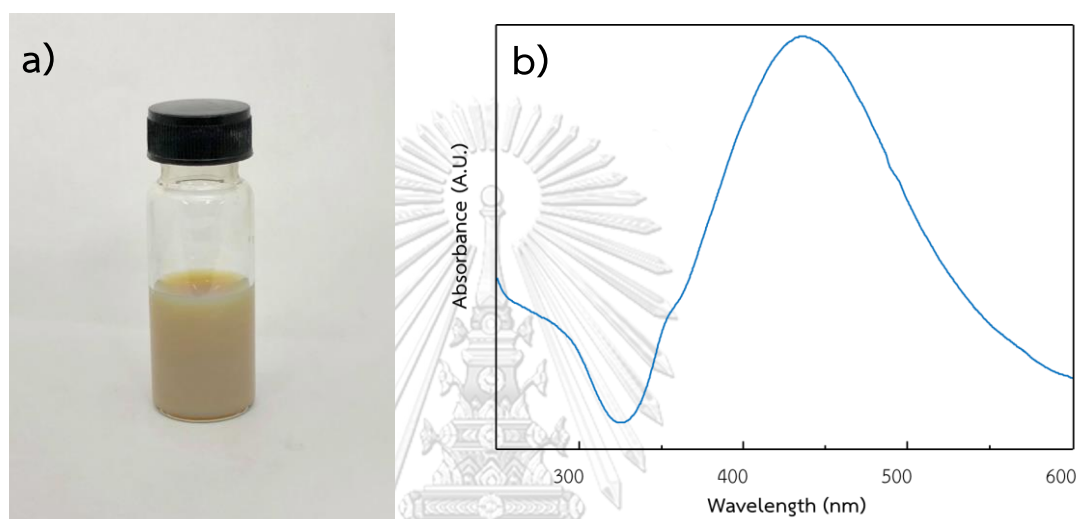


Figure 4.1 (a) synthesized AgNPs colloid and (b) UV-visible spectrum of AgNPs colloid

The yellow-grey colloid of synthesized AgNPs, as shown in Figure 4.1a, has a mass concentration at 0.05 mg/mL. From Figure 4.1b, AgNPs colloid shows the dipole plasmonic band at ~ 430 nm, which indicates that the average size of synthesized AgNPs is approximately 70 nm.⁴² The broad peak also indicates the wide distribution of particles size. The formation of large particles can be observed according to the quadrupole plasmonic band shoulder at ~ 350 nm.⁴³⁻⁴⁴ The obtained diameter size is in the appropriate range for using as SERS substrate because AgNPs with the diameters of 10–100 nm is commonly used as SERS substrates. Too small AgNPs do

not enhance SERS signal effectively because they do not give large enhancement of electric field in visible region compared to IR region.⁴²

4.2 Characterization of thiol-modified AgNP film

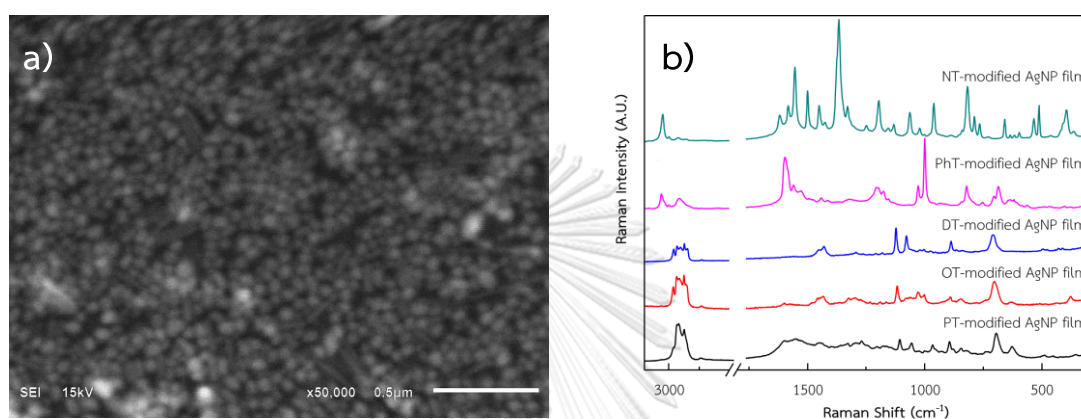


Figure 4.2 (a) SEM image and (b) SERS spectra of thiol-modified AgNP film

To find a suitable substrate for detecting each PAH, the surfaces of AgNPs were functionalized by PT, OT, DT, PhT, and NT. By a LB method, AgNPs were pushed up to the water/hexane interface due to a decrease in polarity of water by an ethanol addition. Thiols in hexane phase also facilitate the movement of AgNPs to the interface *via* a self-assembly force and also reduce the charge on the surface of AgNPs which help increase the miscibility between AgNPs and organic solvent. However, AgNPs are too large which make them cannot enter hexane phase and stuck at the interface resulted in the observed silver mirror film. Without thiols, the AgNPs film cannot be fabricated because thiol acts as a surfactant that induce AgNPs to depart from aqueous phase and assemble at the interface. The characterization of

thiol-modified AgNP film surface was studied by scanning electron microscope (SEM). SEM image (Figure 2a) shows that AgNPs on the film remain in the nanoparticle form which randomly aggregate with each other. SERS spectra collected from each modified film are presented in Figure 2b. Each thiol-modified AgNP film has different characteristic peaks due to the difference in their non-polar structures. Table 4.1 shows band assignments of each thiol-modified AgNP film.



Table 4.1 Band assignments of thiol-modified AgNP films

Substrate	Raman Shift (cm ⁻¹)	Assignment
PT-modified AgNP film	1106, 1056, 966, 894 695, 628	Alkane C–C skeletal vibration C–S stretching
OT-modified AgNP film	1117, 1028 890 702	Alkane C–C skeletal vibration C–C stretching C–S stretching
DT-modified AgNP film	1123, 1078 888 708	Alkane C–C skeletal vibration C–S bending C–S stretching
PhT-modified AgNP film	1597 1206, 1028, 1002 821, 686	Ring C=C stretching =C–H in-plane deformation vibrations C–S stretching
NT-modified AgNP film	1554, 1500 1366 1196 961, 817	Ring C=C stretching C–C stretching C–H bending Ring deformation

4.3 Detection of PAHs using thiol-modified AgNP films

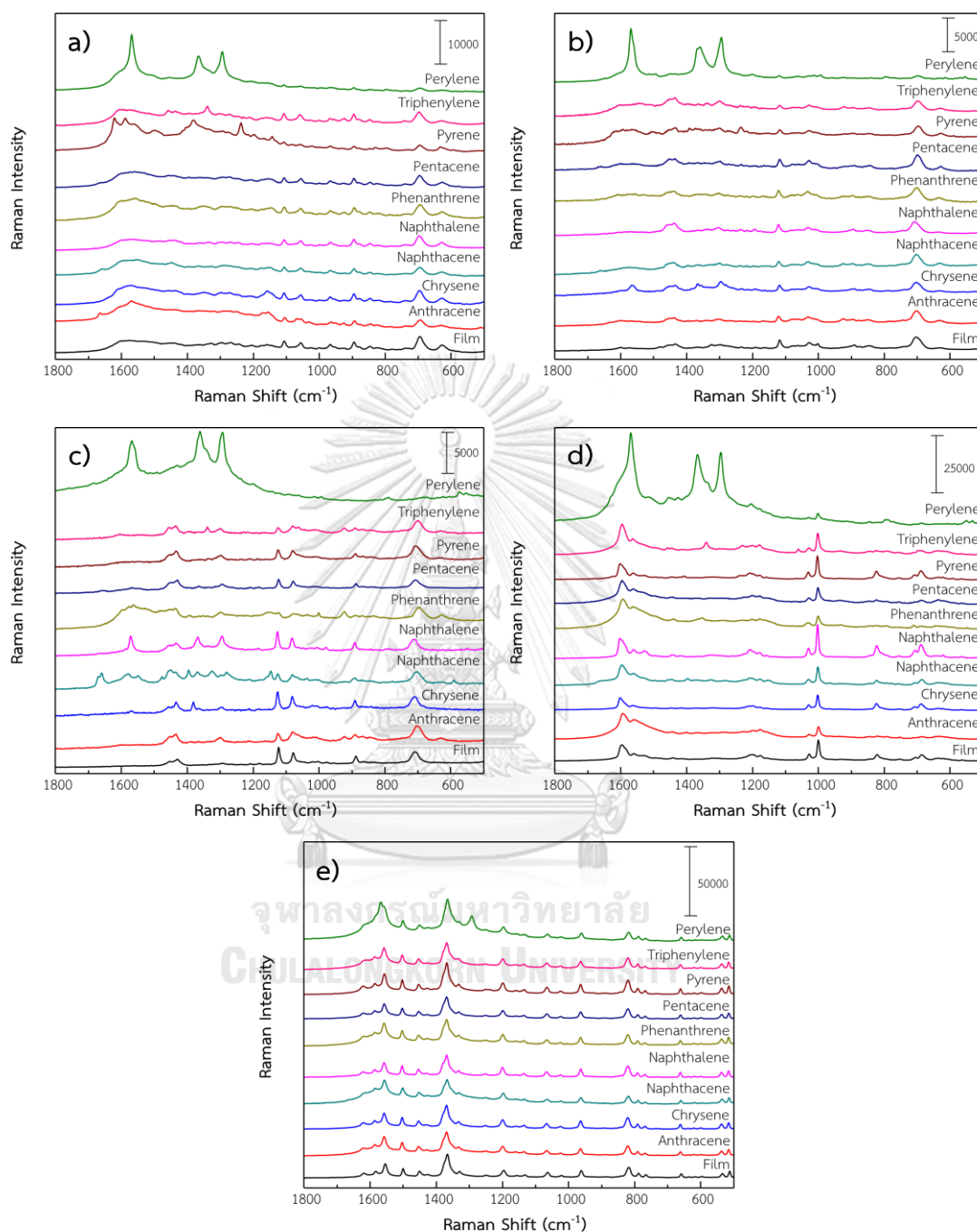


Figure 4.3 SERS spectra of different PAHs at the concentration of 10^{-4} M on (a) PT-, (b) OT-, (c) DT-, (d) PhT-, and (e) NT- modified AgNP films

The functionalization of AgNPs with thiols creates a hot spots with non-polar surfaces which allow the detection of PAHs. Figure 4.3 shows SERS spectra of AgNP film soaked in different PAHs at the concentration of 1.0×10^{-4} M. Thiol group can induce PAHs to adsorb on the nonpolar environment by π - π interactions and/or hydrophobic forces. Different PAHs may be detected by different kinds of thiol-modified AgNP film according to the structure of alkyl/aryl part in thiols (such as chain length, steric effect, and aromaticity). The characteristic peaks and their assignments of each PAH on each substrate are shown in Table 4.2–4.10.



Table 4.2 Band assignments of thiol-modified AgNP films with anthracene

Anthracene on	Raman Shift (cm ⁻¹)	Assignment
PT-modified AgNP film	1569	C–C stretching
	692	C–S stretching
OT-modified AgNP film	1121	Alkane C–C skeletal vibration
	701	C–S stretching
DT-modified AgNP film	1436	C=C–C aromatic vibration
	1080	Alkane C–C skeletal vibration
	699	C–S stretching
PhT-modified AgNP film	1593	C=C–C aromatic vibration
	1000	=C–H in-plane deformation
NT-modified AgNP film	1557, 1503, 1453	Ring C=C stretching
	1369	C–C stretching
	1199, 1066	In-plane C–H bending
	964	Out-of-plane C–H bending
	820	Ring deformation

Table 4.3 Band assignments of thiol-modified AgNP films with chrysene

Chrysene on	Raman Shift (cm ⁻¹)	Assignment
PT-modified AgNP film	1568, 895	C–C stretching
	695	C–S stretching
OT-modified AgNP film	1565,	C–C stretching
	1296	C–H bending
	1118	Alkane C–C skeletal vibration
	702	C–S stretching
DT-modified AgNP film	1432	C=C–C aromatic vibration
	1382	Skeletal ring vibration
	1126, 1081	Alkane C–C skeletal vibration
	890, 711	C–S stretching
PhT-modified AgNP film	1600	C=C–C aromatic vibration
	1002	=C–H in-plane deformation
	823, 688	C–S stretching
NT-modified AgNP film	1557, 1503, 1453	Ring C=C stretching
	1369	C–C stretching
	1199	C–H bending
	821	Ring deformation

Table 4.4 Band assignments of thiol-modified AgNP films with naphthacene

Naphthacene on	Raman Shift (cm ⁻¹)	Assignment
PT-modified AgNP film	1558, 894	C–C stretching
	696	C–S stretching
OT-modified AgNP film	1565,	C–C stretching
	1296	C–H bending
	1118	Alkane C–C skeletal vibration
	702	C–S stretching
DT-modified AgNP film	1577, 1449	C–C ring stretching
	1396	Skeletal ring vibration
	1081	Alkane C–C skeletal vibration
	702	C–S stretching
PhT-modified AgNP film	1597	C=C–C aromatic vibration
	1002	=C–H in-plane deformation
	823, 687	C–S stretching
NT-modified AgNP film	1556, 1501, 1452	Ring C=C stretching
	1367	C–C stretching
	1197, 1064	In-plane C–H bending
	962	Out-of-plane C–H bending
	818	Ring deformation

Table 4.5 Band assignments of thiol-modified AgNP films with naphthalene

Naphthalene on	Raman Shift (cm ⁻¹)	Assignment
PT-modified AgNP film	1106	Alkane C–C skeletal vibration
	895	C–C stretching
	696	C–S stretching
OT-modified AgNP film	1436	C–H bending
	1121	Alkane C–C skeletal vibration
	1031	=C–H in-plane deformation
	708	C–S stretching
DT-modified AgNP film	1434	C=C–C aromatic vibration
	1294	C–H bending
	1126, 1081	Alkane C–C skeletal vibration
	891, 696	C–S stretching
PhT-modified AgNP film	1602	C=C–C aromatic vibration
	1003	=C–H in-plane deformation
	823, 688	C–S stretching
NT-modified AgNP film	1557 1503, 1454	Ring C=C stretching
	1369	C–C stretching
	1200	In-plane C–H bending
	963	Out-of-plane C–H bending
	820	Ring deformation

Table 4.6 Band assignments of thiol-modified AgNP films with phenanthrene

Phenanthrene on	Raman Shift (cm ⁻¹)	Assignment
PT-modified AgNP film	1571, 894	C–C stretching
	694	C–S stretching
OT-modified AgNP film	1440	C–C stretching
	1120	Alkane C–C skeletal vibration
	708	C–S stretching
DT-modified AgNP film	696	C–S stretching
PhT-modified AgNP film	1594	C=C–C aromatic vibration
	1001	=C–H in-plane deformation
NT-modified AgNP film	1558 1503, 1453	Ring C=C stretching
	1369	C–C stretching
	1199	C–H bending
	820	Ring deformation

Table 4.7 Band assignments of thiol-modified AgNP films with pentacene

Pentacene on	Raman Shift (cm ⁻¹)	Assignment
PT-modified AgNP film	1559, 894	C–C stretching
	696	C–S stretching
OT-modified AgNP film	1435	C–C stretching
	1118	Alkane C–C skeletal vibration
	1031	=C–H in-plane deformation
	701	C–S stretching
DT-modified AgNP film	1431	C=C–C aromatic vibration
	1123, 1080	Alkane C–C skeletal vibration
	888, 708	C–S stretching
PhT-modified AgNP film	1595	C=C–C aromatic vibration
	1001	=C–H in-plane deformation
NT-modified AgNP film	1556, 1502, 1453	Ring C=C stretching
	1368	C–C stretching
	1198	C–H bending
	820	Ring deformation

Table 4.8 Band assignments of thiol-modified AgNP films with perylene

Perylene on	Raman Shift (cm ⁻¹)	Assignment
PT-modified AgNP film	1568, 1367	C–C stretching
	1299	C–H bending
OT-modified AgNP film	1569, 1367	C–C stretching
	1294	C–H bending
DT-modified AgNP film	1567, 1360	C–C stretching
	1293	C–H bending
PhT-modified AgNP film	1569, 1367	C–C stretching
	1297	C–H bending
	1002	=C–H in-plane deformation vibrations
NT-modified AgNP film	1567, 1366	C–C stretching
	1500, 1450	Ring C=C stretching
	1293	C–H bending
	1197	C–H bending

Table 4.9 Band assignments of thiol-modified AgNP films with pyrene

Pyrene on	Raman Shift (cm ⁻¹)	Assignment
PT-modified AgNP film	1621	C=C ring stretching
	1588	C–C stretching
	1380	Skeletal ring vibration
	1238	=C–H in-plane deformation vibration
	695	C–S stretching
OT-modified AgNP film	1620	C=C ring stretching
	1380	Skeletal ring vibration
	697	C–S stretching
DT-modified AgNP film	1125, 1080	Alkane C–C skeletal vibration
	890, 707	C–S stretching
PhT-modified AgNP film	1602	C=C–C aromatic vibration
	1003	=C–H in-plane deformation
	823, 689	C–S stretching
NT-modified AgNP film	1556, 1502, 1453	Ring C=C stretching
	1368	C–C stretching
	1199	C–H bending
	820	Ring deformation

Table 4.10 Band assignments of thiol-modified AgNP films with triphenylene

Triphenylene on	Raman Shift (cm ⁻¹)	Assignment
PTmodified AgNP film	1339 1107 895 697	C=C-C aromatic vibration Alkane C-C skeletal vibration C-C stretching C-S stretching
OT-modified AgNP film	1340 1031 700	C=C-C aromatic vibration =C-H in-plane deformation vibrations C-S stretching
DT-modified AgNP film	1457, 1339 698	C=C-C aromatic vibration C-S stretching
PhT-modified AgNP film	1596, 1565, 1367 1298 1002	C=C-C aromatic vibration C-C stretching =C-H in-plane deformation vibrations
NT-modified AgNP film	1557, 1502, 1453 1368 1199, 1066, 963 820	Ring C=C stretching C-C stretching C-H bending Ring deformation

The characteristic peaks of perylene can be obviously observed on PT-, OT-, DT-, and PhT-modified AgNP films with the Raman shift at 1568 and 1367 cm^{-1} correspond to C–C stretching, and 1299 cm^{-1} corresponding to C–H bending. The intensity of characteristic peaks from perylene are higher than other PAHs because the vibration mode of these 3 peaks are a totally symmetric vibration mode, which usually gives the stronger Raman intensity.⁴⁵⁻⁴⁷ Some of pyrene characteristic peaks are also a totally symmetric vibration modes which resulted in the stronger Raman intensity.⁴⁸ Other PAHs characteristic peaks cannot be seen directly from the spectra because of the peak overlapping between substrate and PAH, which may happen because PAHs have no specific functional groups that are different from substrate. So, we proposed mathematical method to get more effective data analysis

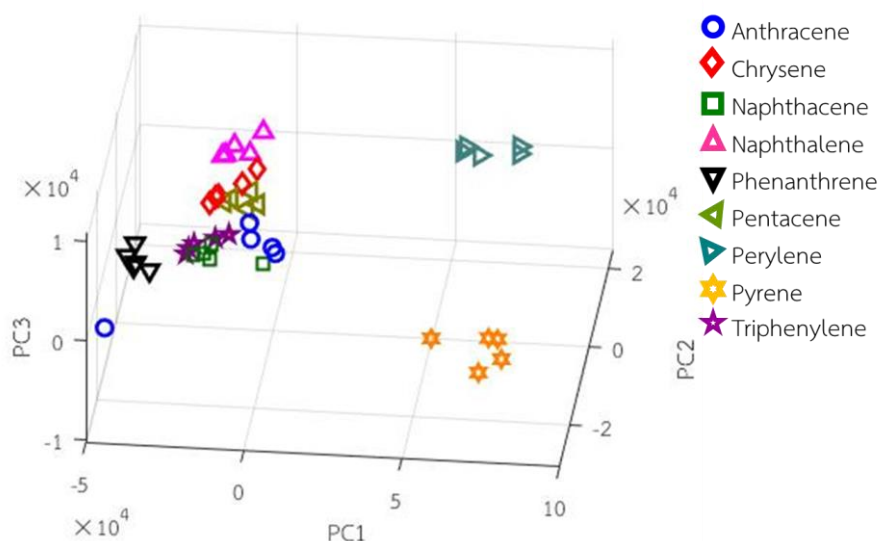


Figure 4.4 PCA plots of 9 PAHs on PT-modified AgNP film

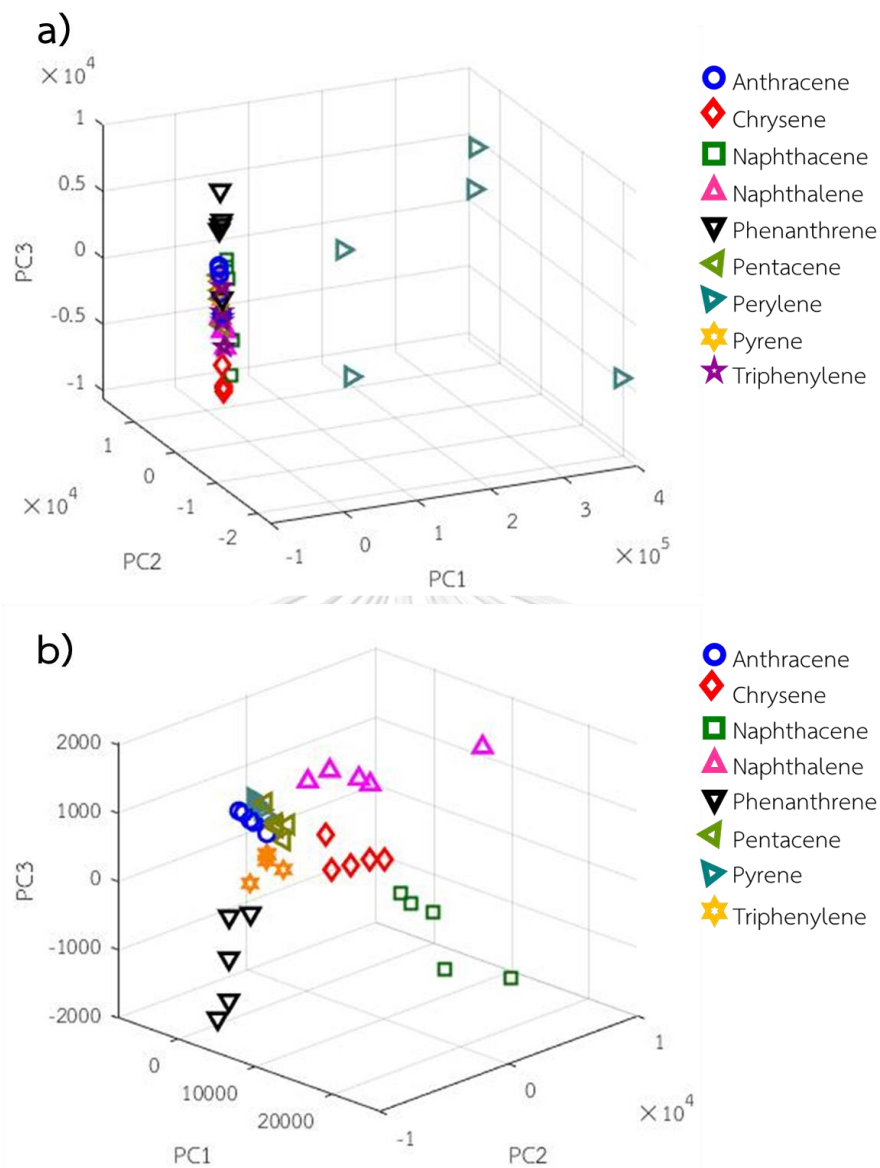


Figure 4.5 PCA plots of 9 PAHs on PhT-modified AgNP film (a) full plot (b) expanded plot.

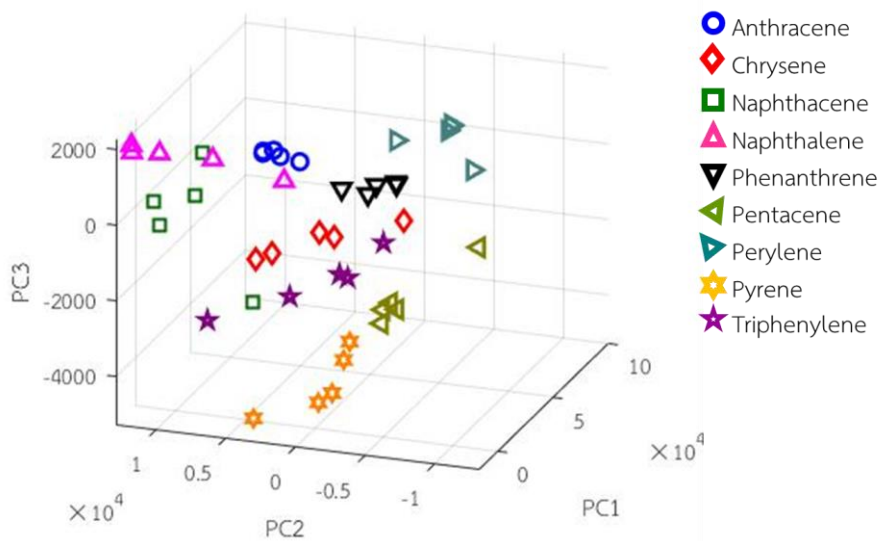


Figure 4.6 PCA plots of 9 PAHs on OT-modified AgNP film

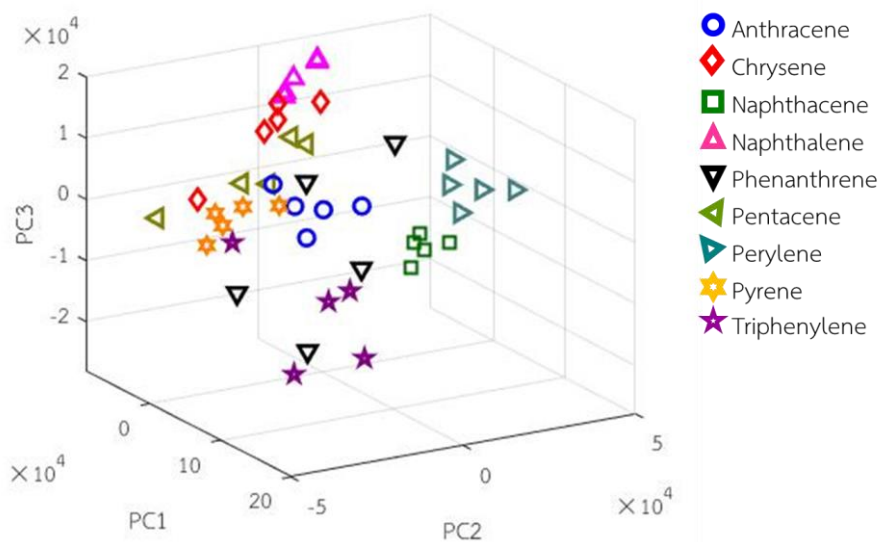


Figure 4.7 PCA plots of 9 PAHs on NT-modified AgNP film.

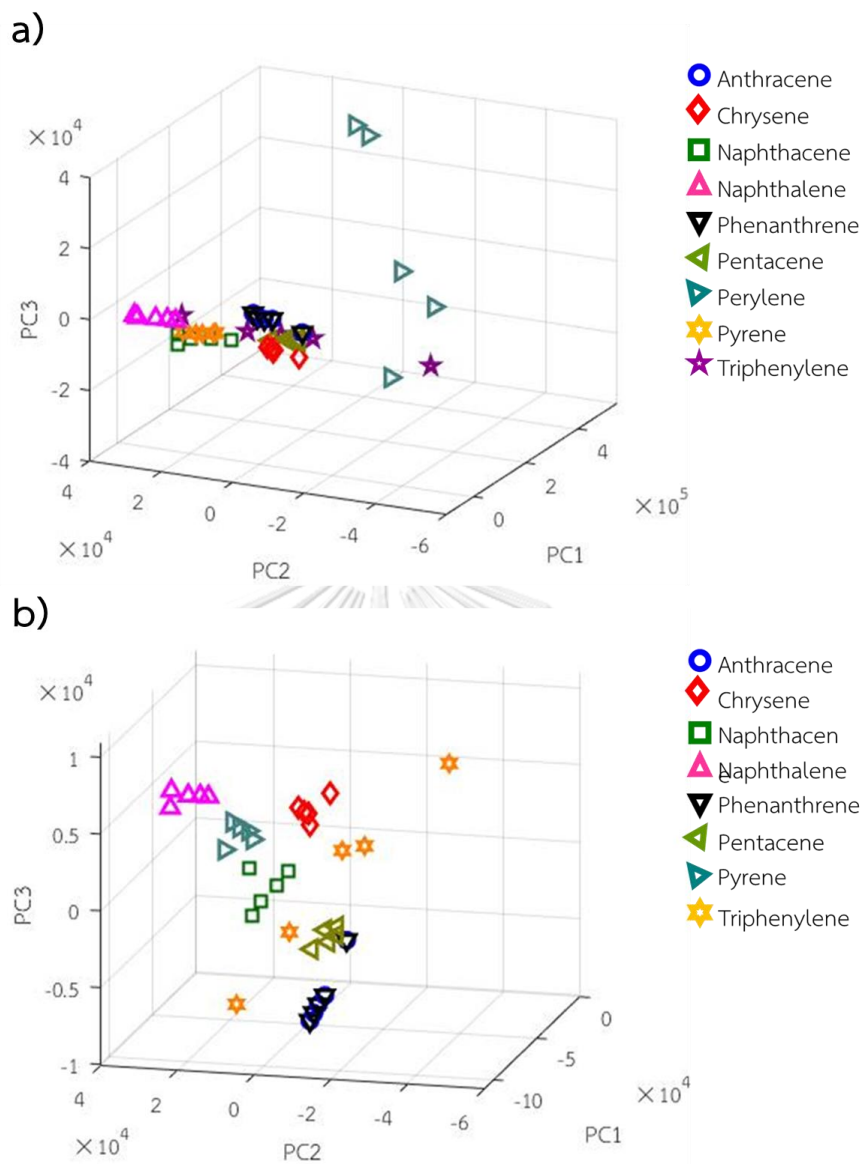


Figure 4.8 PCA plots of 9 PAHs on PhT-modified AgNP film (a) full plot (b) expanded plot.

To consider the appropriate pairs of substrates and PAHs, the data were analyzed with PCA and cluster separation, respectively. In this research, the reduced data matrices are in the form of scores with three PCs. The obtained PCA plots of

first three PCs (Figure 4.4–4.8) show that groups of PAHs separate from group of bare substrates. However, using different PCs normally gives different results so the cluster separation index (CSI) is proposed for PCs selection. In this work, we used Davies Bouldin Index (DBI) which is one of the common CSIs used for results validation. For DBI, the lower value indicates a better separation between 2 classes.^{36, 49-50} From overall DBI results (Table 4.3), PT-, PhT-, and NT-modified AgNP films provide effective results. For NT- and PhT-modified AgNP film cases, the aromatic ring in the structure of substrate and analyte creates π - π interaction, which makes analyte attached into the hot spot area resulted in the signal enhancement. Even though PAHs structure promotes the π - π interaction with substrate as they consist of several aromatic rings. Nevertheless, in some cases, the distance between hot spot and PAH shows a more dominant effect to the signal enhancement than the effect of π - π interaction. The mentioned case can be found in pyrene and phenanthrene on PT-modified AgNP film which have a lower DBI value when compare with NT- and PhT-modified AgNP film.

Table 4.11 DBI value of different PAHs on different thiol-modified AgNP films

	DT	OT	PT	NT	PhT
Anthracene	1.202	0.731	0.889	0.282	0.582
Chrysene	0.495	1.947	1.584	0.248	0.364
Naphthacene	0.318	0.384	0.677	0.153	0.361
Naphthalene	0.592	0.584	0.803	0.116	0.692
Phenanthrene	0.583	0.496	0.338	0.468	0.582
Pentacene	0.762	0.559	0.836	0.370	0.348
Perylene	0.139	0.292	0.127	0.119	0.108
Pyrene	0.861	0.710	0.136	0.282	2.923
Triphenylene	1.565	2.754	0.773	0.314	1.246

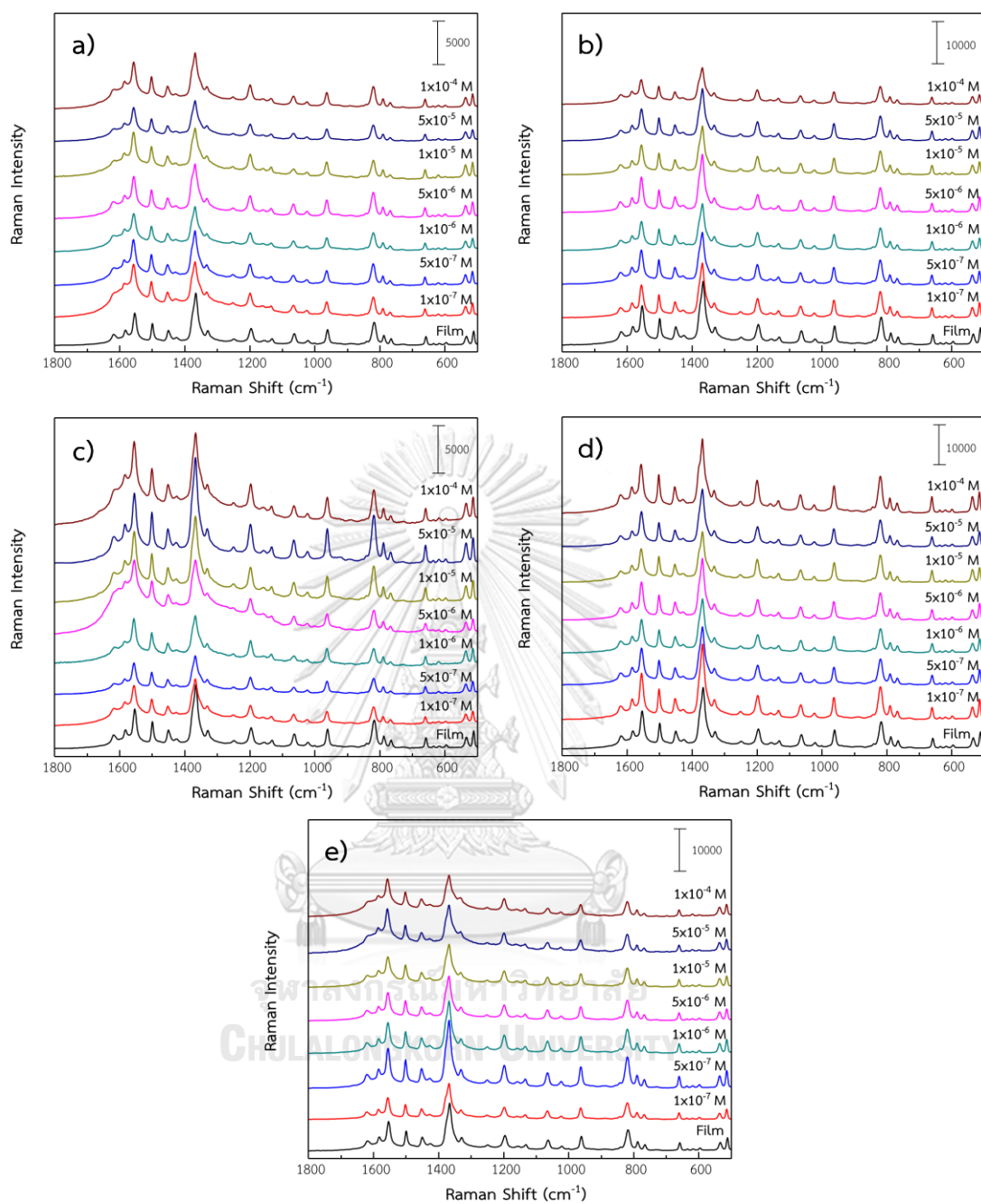


Figure 4.9 SERS spectra of NT-modified AgNP films with (a) anthracene, (b) chrysene, (c) naphthacene, (d) naphthalene, and (e) triphenylene.

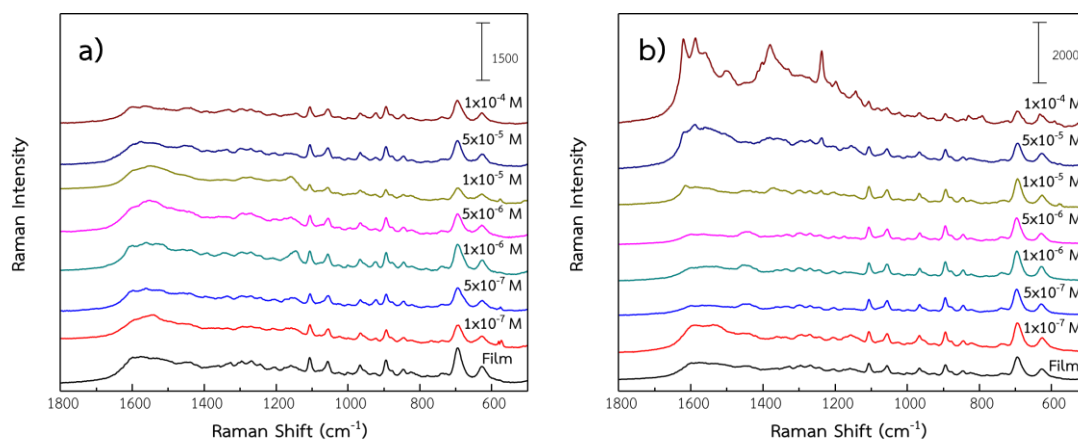


Figure 4.10 SERS spectra of PT-modified AgNP films with (a) phenanthrene and (b) pyrene.

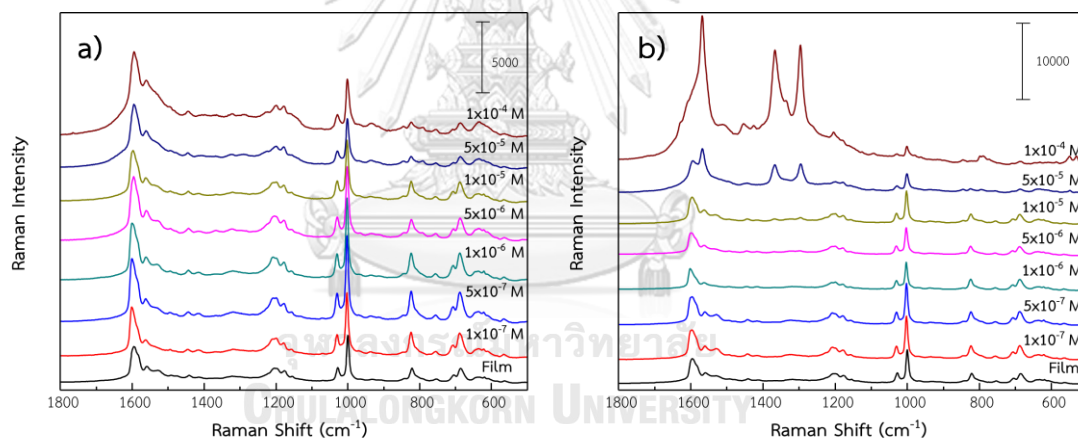


Figure 4.11 SERS spectra of PhT-modified AgNP films with (a) pentacene and (b) perylene.

From Table 4.11, the most appropriate pairs of substrate and PAH are; anthracene, chrysene, naphthacene, naphthalene, and triphenylene with NT-modified AgNP film; pentacene and perylene with PhT-modified AgNP film; and

pyrene and phenanthrene with PT-modified AgNP film. Then, we detect each PAH with different concentrations (1×10^{-4} , 5×10^{-5} , 1×10^{-5} , 5×10^{-6} , 1×10^{-6} , 5×10^{-7} , and 1×10^{-7}) on its suitable substrate to determine the sensitivity of detection. Figure 4.9, 4.10, and 4.11 show the spectra of each PAH with different concentrations on the substrate. From the result, only some PAHs can be determined directly as their characteristic peaks can be obviously observed from raw spectra.

The conventional way for quantitative analysis is to determine the relationship between concentration and Raman intensity by finding the relative relationship between the intensity of selected PAH characteristic peak and the intensity of selected reference peak. However, the relationship between Raman intensity and concentration is hard to determine directly from raw spectra because some characteristic peaks of PAH is hard to be observed directly. Therefore, in this study, the quantitative analysis was performed by the help of mathematical procedures because we cannot determine which peak ratios should be used to create a linear calibration curve for determining the amount of PAH straight from raw spectra.

Partial least square (PLS) regression is one of supervised pattern recognition mathematical model for predicting the data which has large number of factors. In this work, PLS was used for building calibration between Raman intensity and PAH concentration using whole spectrum (in the region between $500\text{--}1800\text{ cm}^{-1}$) to analyze for more effective analysis.

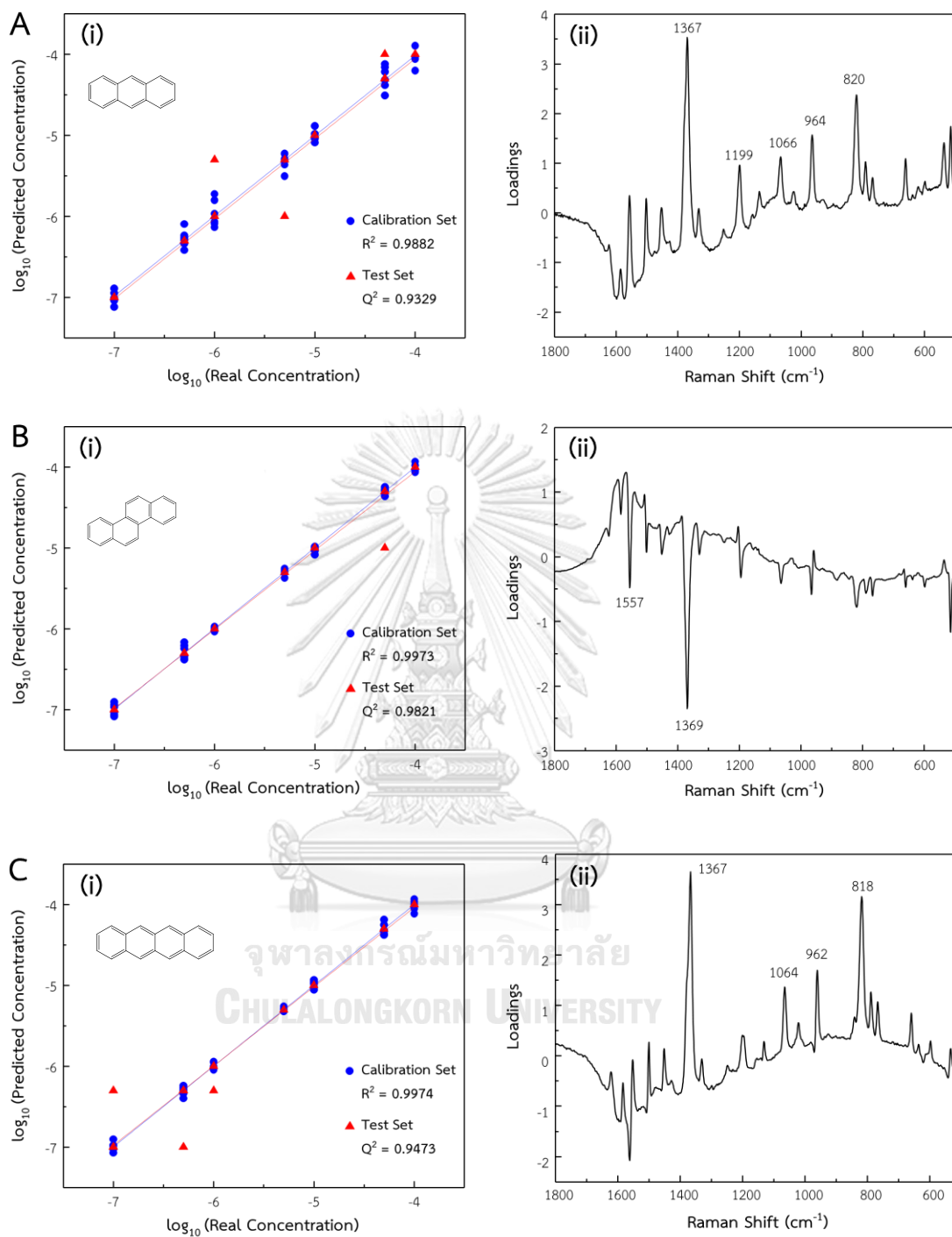


Figure 4.12 (i) PLS models and (ii) first loading plots of NT-modified AgNP films with (A) anthracene, (B) chrysene, and (C) naphthacene.

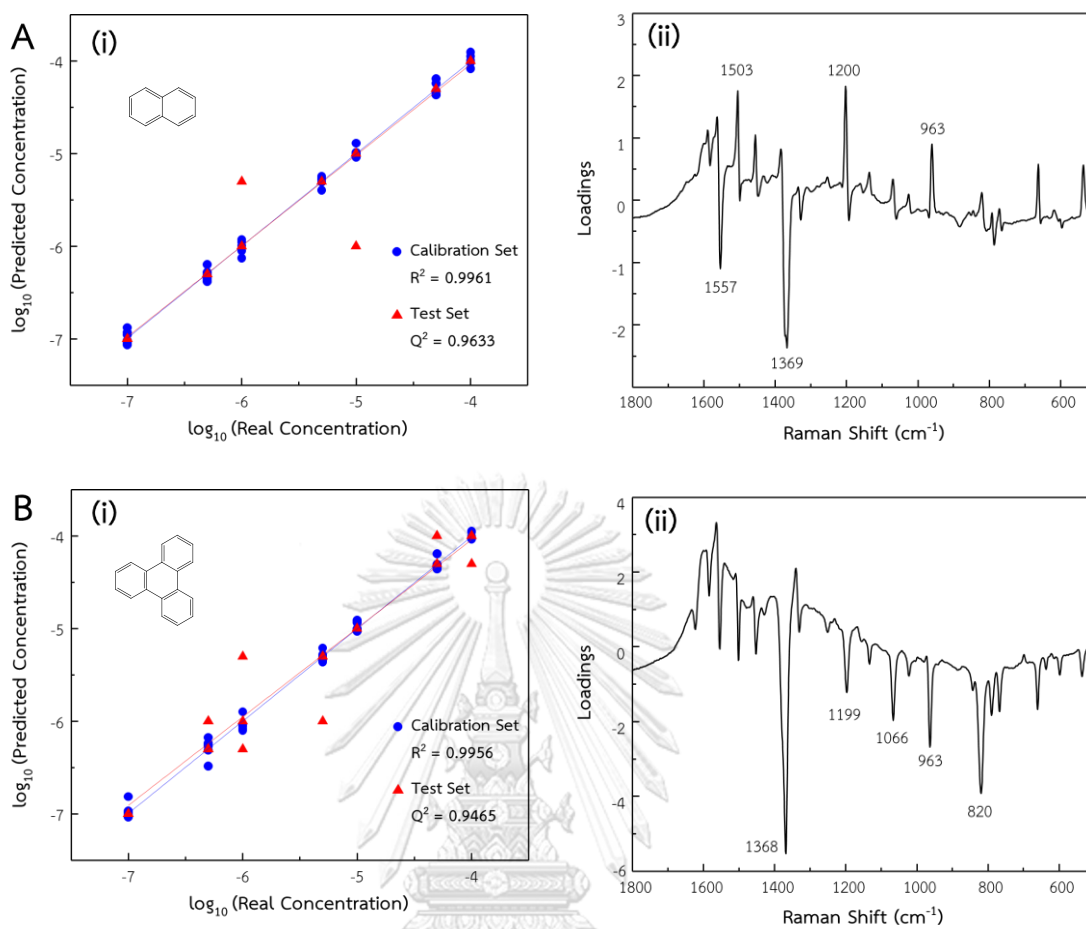


Figure 4.13 (i) PLS models and (ii) first loading plots of NT-modified AgNP films with

(A) naphthalene, and (B) triphenylene.

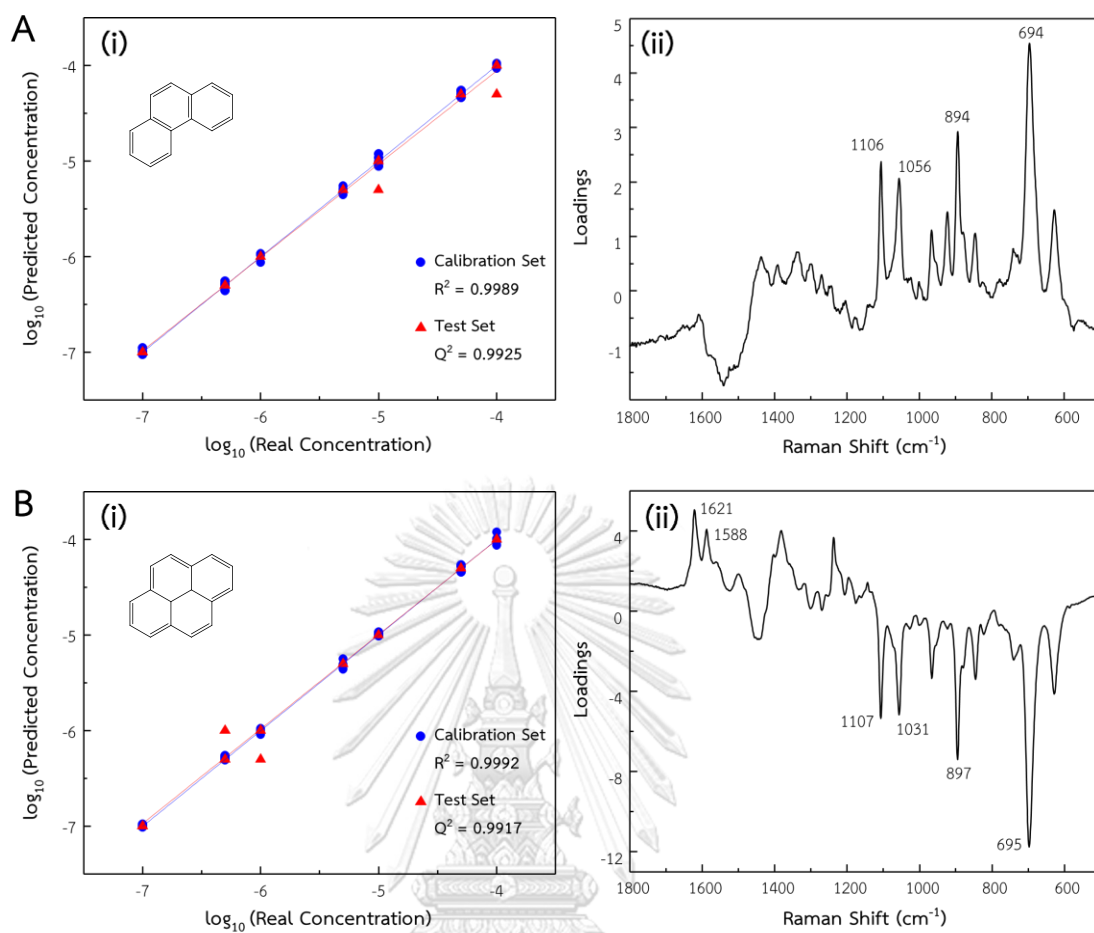


Figure 4.14 (i) PLS models and (ii) first loading plots of PT-modified AgNP films with

(A) phenanthrene and (B) pyrene.

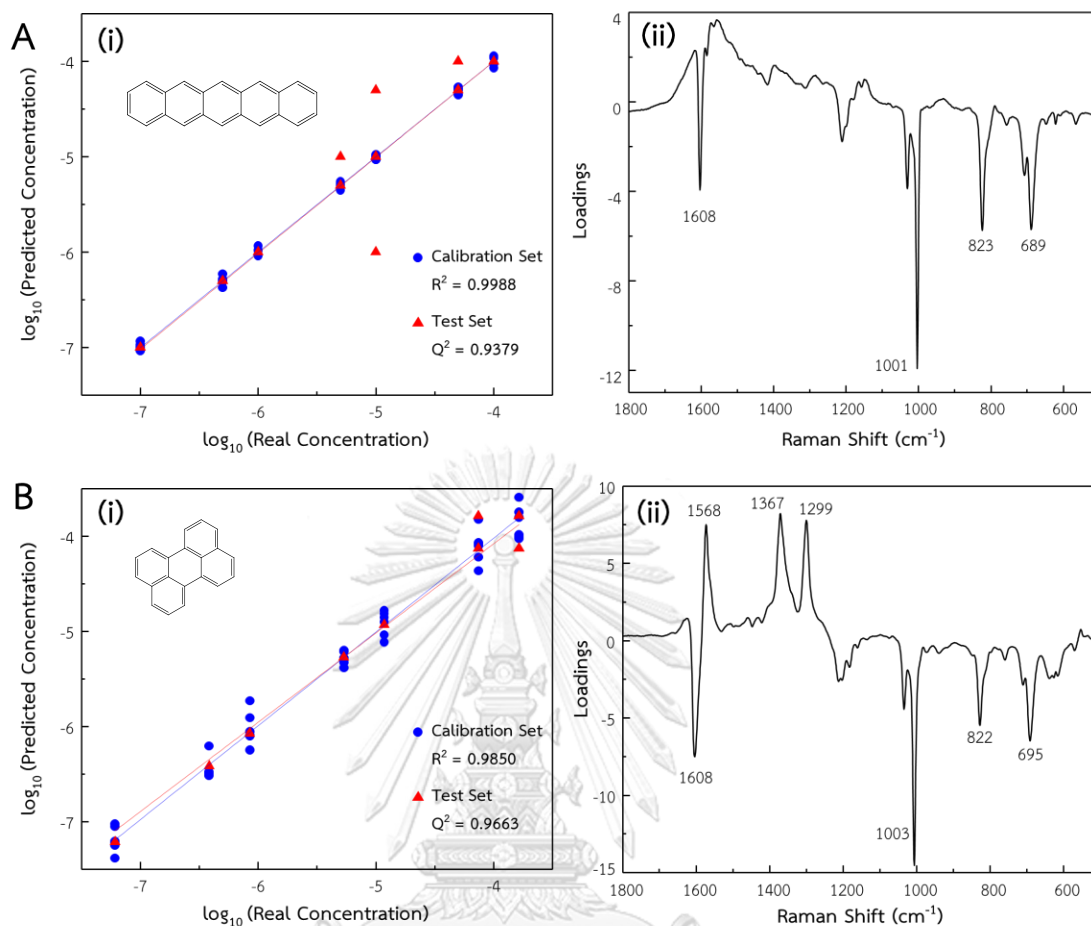


Figure 4.15 (i) PLS models and (ii) first loading plots of PhT-modified AgNP films with (A) pentacene and (B) perylene.

The obtained results show a straight relationship between real concentration and predicted concentration (Figure 4.12–4.15). The obtained PLS model was then validated by using leave one out cross validation (LOOCV) technique. Briefly, one measurement was used as test set to validate the model built from the calibration set of the remaining measurements, the R^2 obtained from LOOCV calibration curve will be assigned as Q^2 . The obtained R^2 value and Q^2 value are shown in Table 4.12. From Figure 4.9–4.11 (i), the cross-validation models (red triangle) indicates that the

obtained PLS model can predict the concentration effectively as their Q^2 is higher than 0.98 with the low distributed cross-validation models. The higher R^2 and Q^2 value indicating the more effective prediction of the achieved PLS and cross-validation models. To determine the relationship of peaks that are affected by the concentration, the first loading of PLS model was plot against wavenumber. The sharp peaks shown in Figure 4.9–4.11 (ii) indicate that the peak are affected when the concentration changed. The peaks that are in negative area normally belong to substrate. An increase in PAH concentration hinders the substrate surface resulted in a decrease in the peak intensity of substrate in raw spectra. The peaks in positive area normally belong to PAH as the peak intensity of PAH in raw spectra increase when PAH concentration increase. The intensity of each peak obtained from first loading plot are in the same trend as the achieved results.

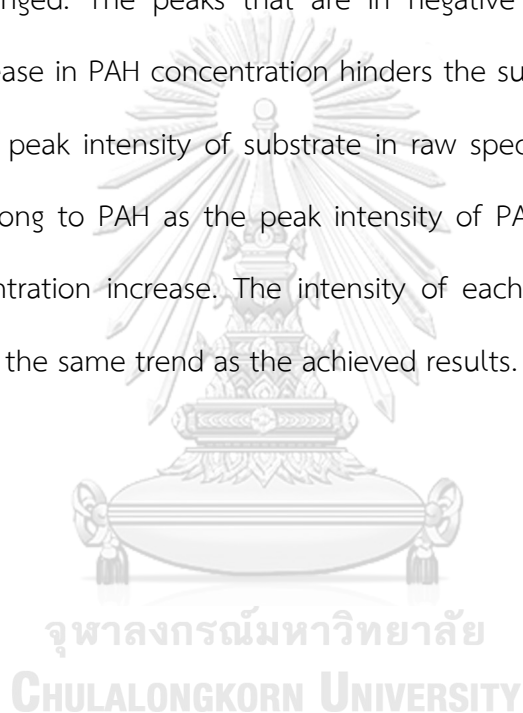


Table 4.12 R^2 of calibration curve and Q^2 of LOOCV for the determination of different PAHs

PAH	R^2	Q^2
Anthracene	0.9882	0.9329
Chrysene	0.9973	0.9821
Naphthacene	0.9974	0.9473
Naphthalene	0.9961	0.9633
Phenanthrene	0.9989	0.9925
Pentacene	0.9988	0.9379
Perylene	0.9862	0.9663
Pyrene	0.9992	0.9917
Triphenylene	0.9956	0.9465

4.4 Determination of PAH in two-PAHs mixture

After evaluating the ability of substrate for the detection of PAHs and getting the suitable substrate for each PAH, mixtures of 2 different PAHs (the analyzed PAH with 5 various concentrations and the interfering PAH with constant concentration, as shown in Table 3.1), were exploited as more complicated systems. The systems were created to determine the sensitivity of the substrate to detect analyzed PAH in the presence of the interfering PAH. According to the DBI value (Table 4.11), the NT- and PhT-modified AgNP films were selected as a substrate due to their better efficiency for overall detection compare with other thiol-modified AgNP films.

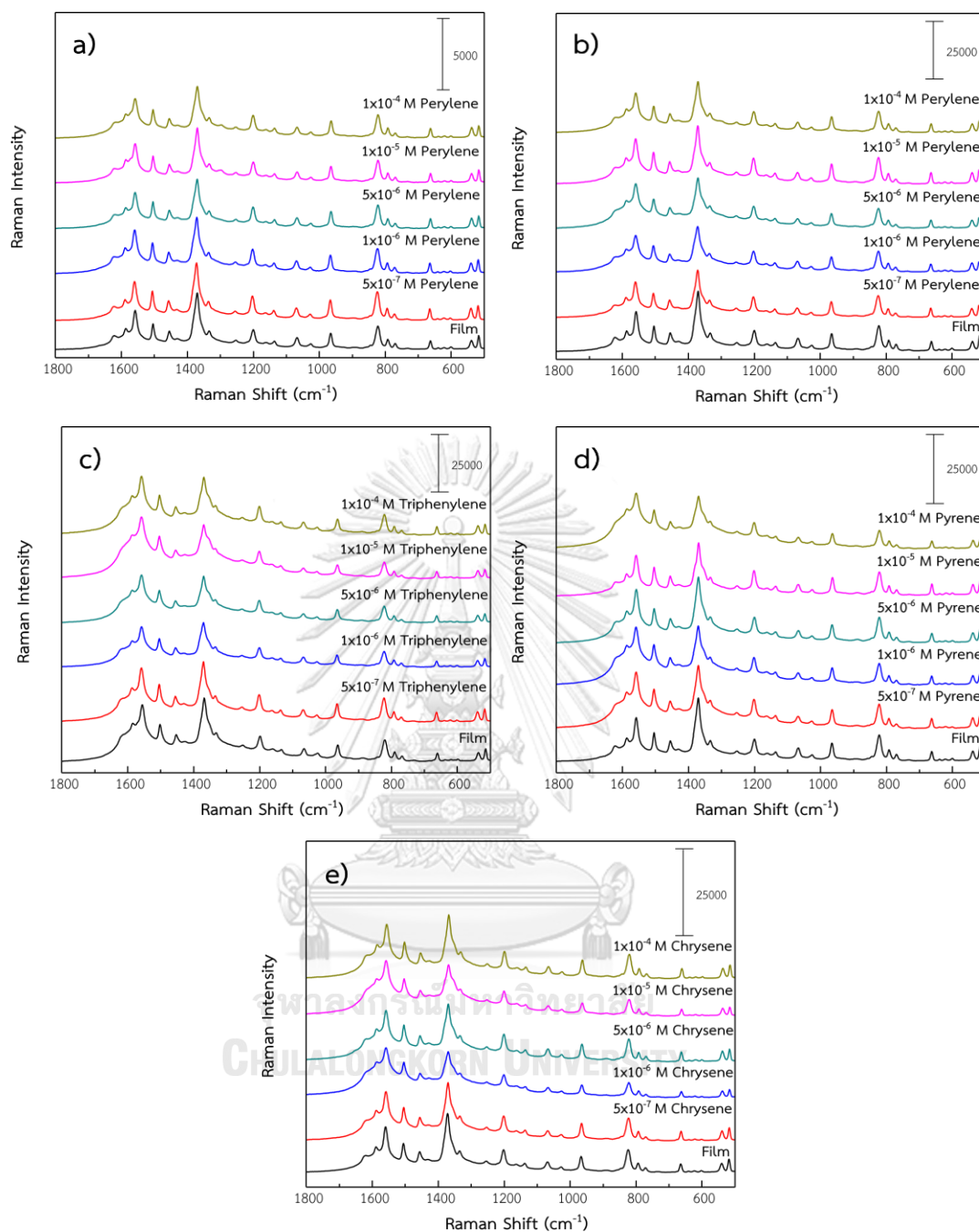


Figure 4.16 SERS spectra of NT-modified AgNP films with (a) perylene in the presence of chrysene, (b) perylene in the presence of pyrene, (c) triphenylene in the presence of chrysene, (d) pyrene in the presence of pentacene, and (e) chrysene in the presence of naphthacene.

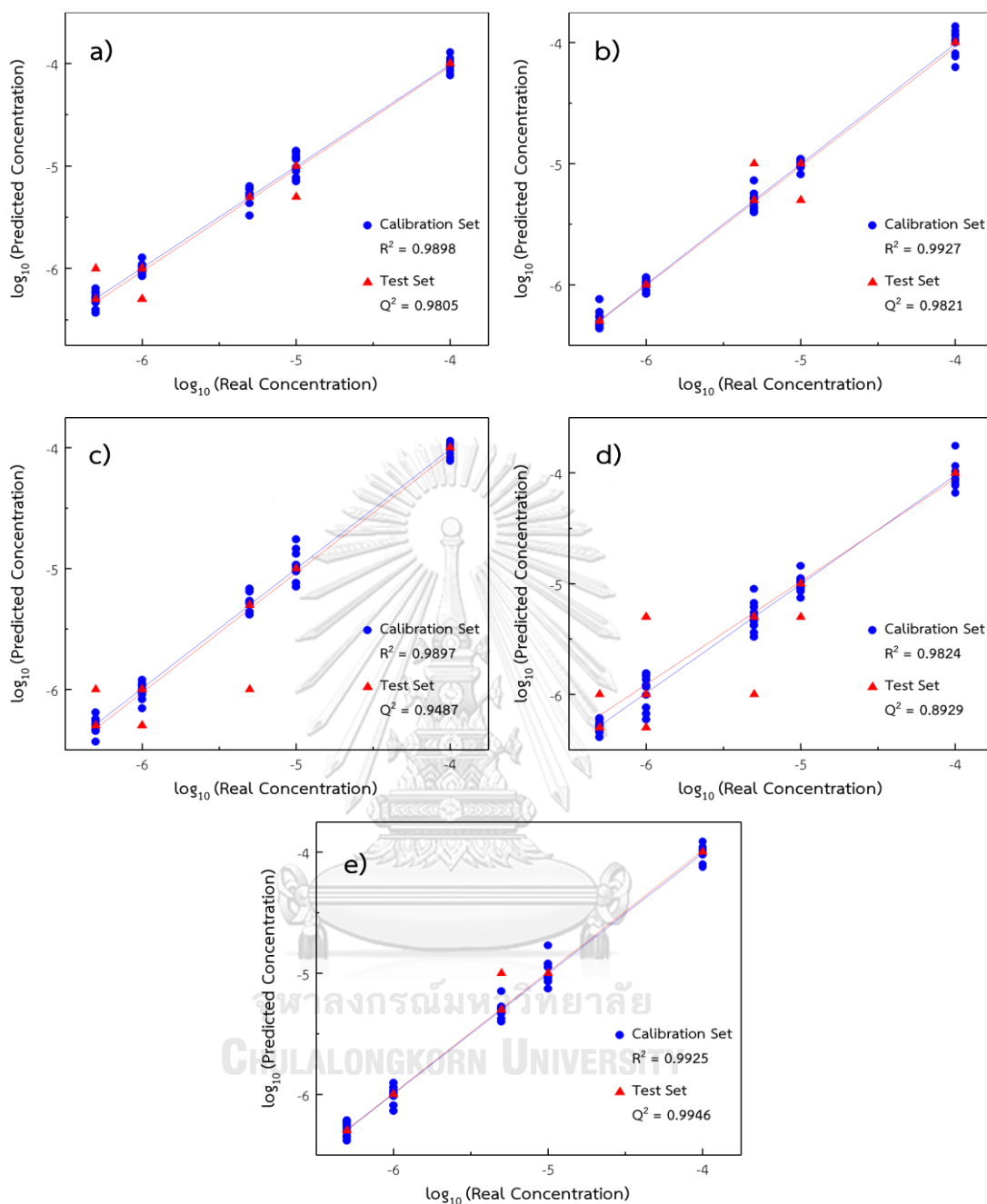


Figure 4.17 PLS models for NT-modified AgNP films with (a) perylene in the presence of chrysene, (b) perylene in the presence of pyrene, (c) triphenylene in the presence of chrysene, (d) pyrene in the presence of pentacene, and (e) chrysene in the presence of naphthacene.

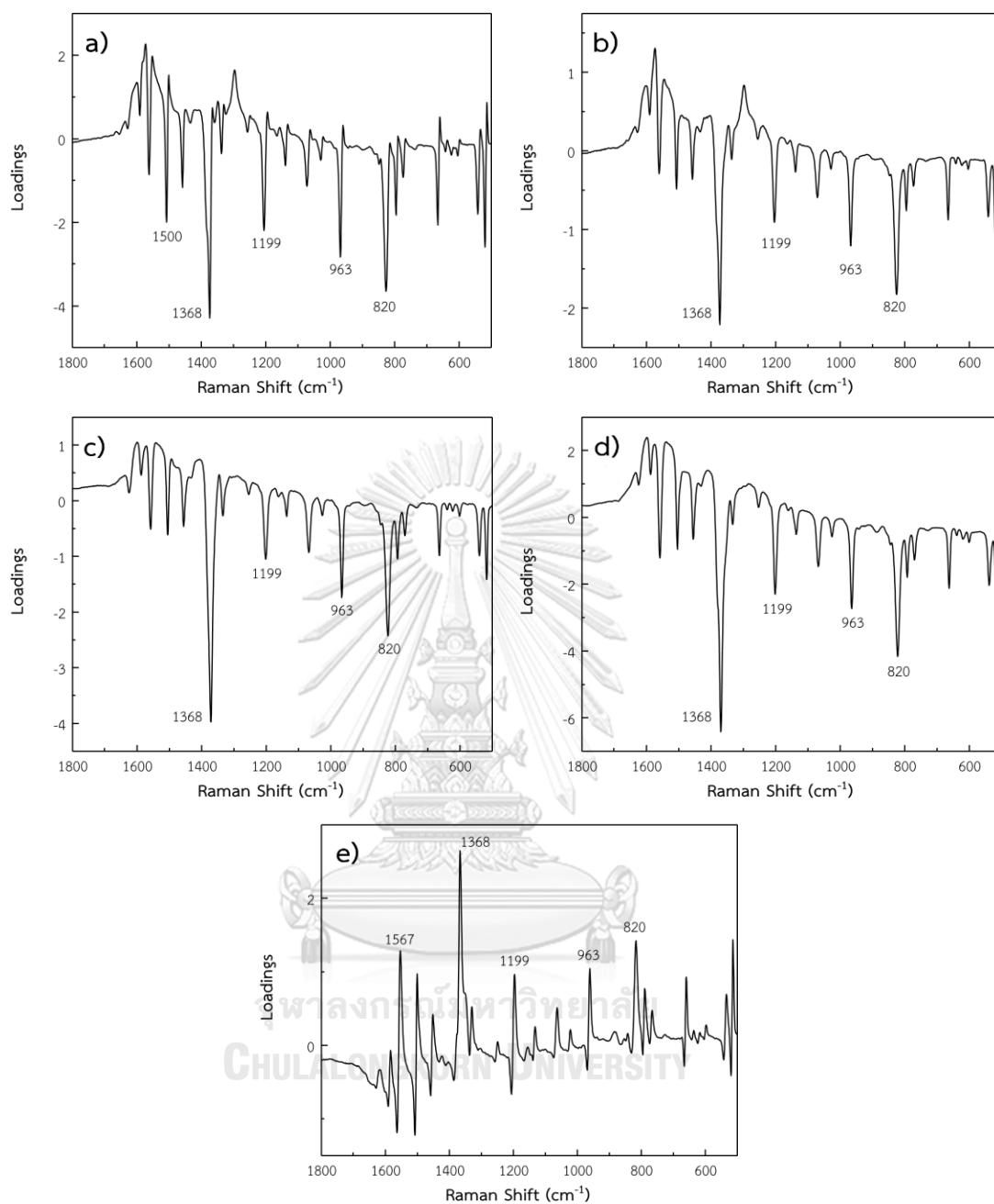


Figure 4.18 First loading plots of NT-modified AgNP films with (a) perylene in the presence of chrysene, (b) perylene in the presence of pyrene, (c) triphenylene in the presence of chrysene, (d) pyrene in the presence of pentacene, and (e) chrysene in the presence of naphthacene.

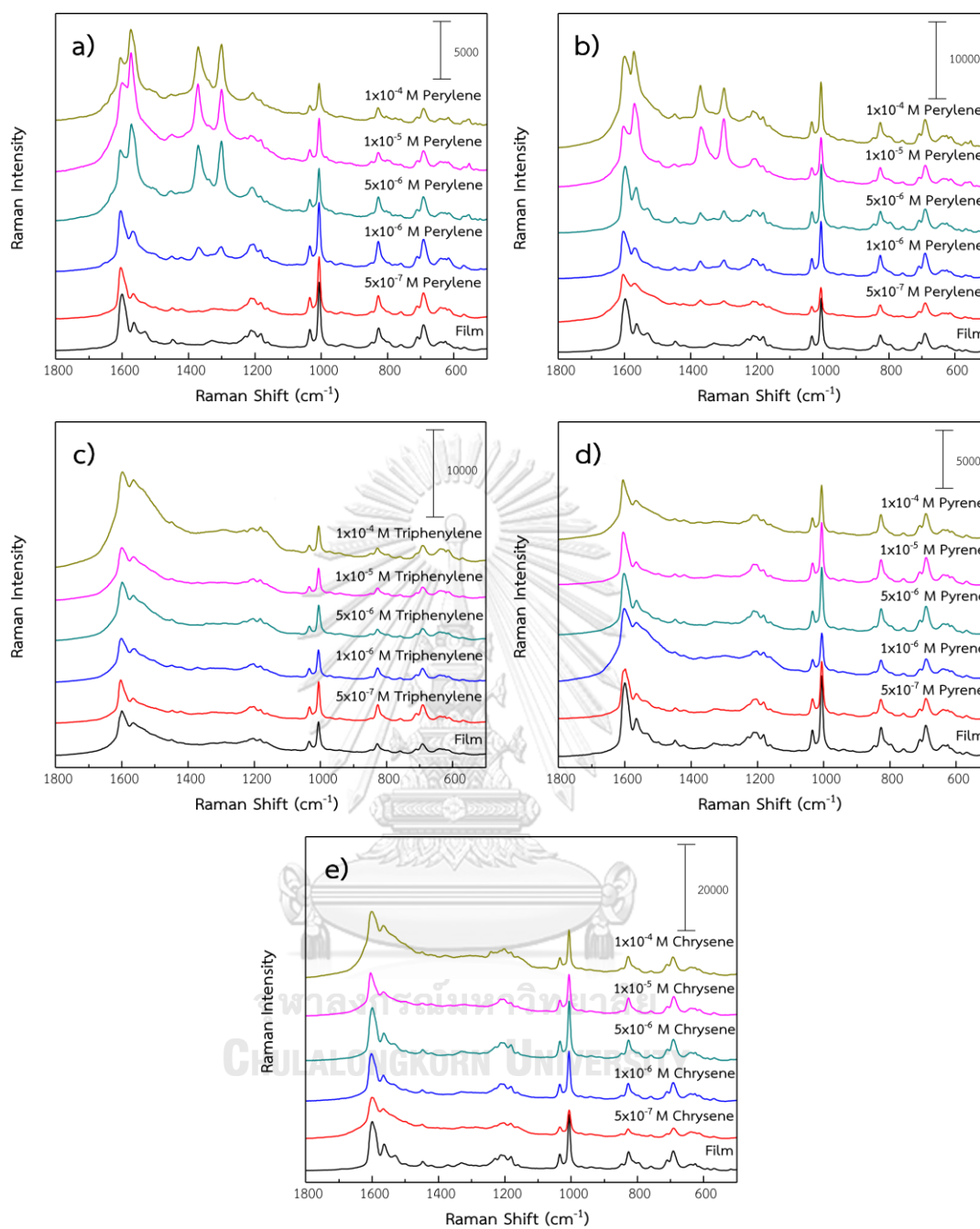


Figure 4.19 SERS spectra of PhT-modified AgNP films with (a) perylene in the presence of chrysene, (b) perylene in the presence of pyrene, (c) triphenylene in the presence of chrysene, (d) pyrene in the presence of pentacene, and (e) chrysene in the presence of naphthacene.

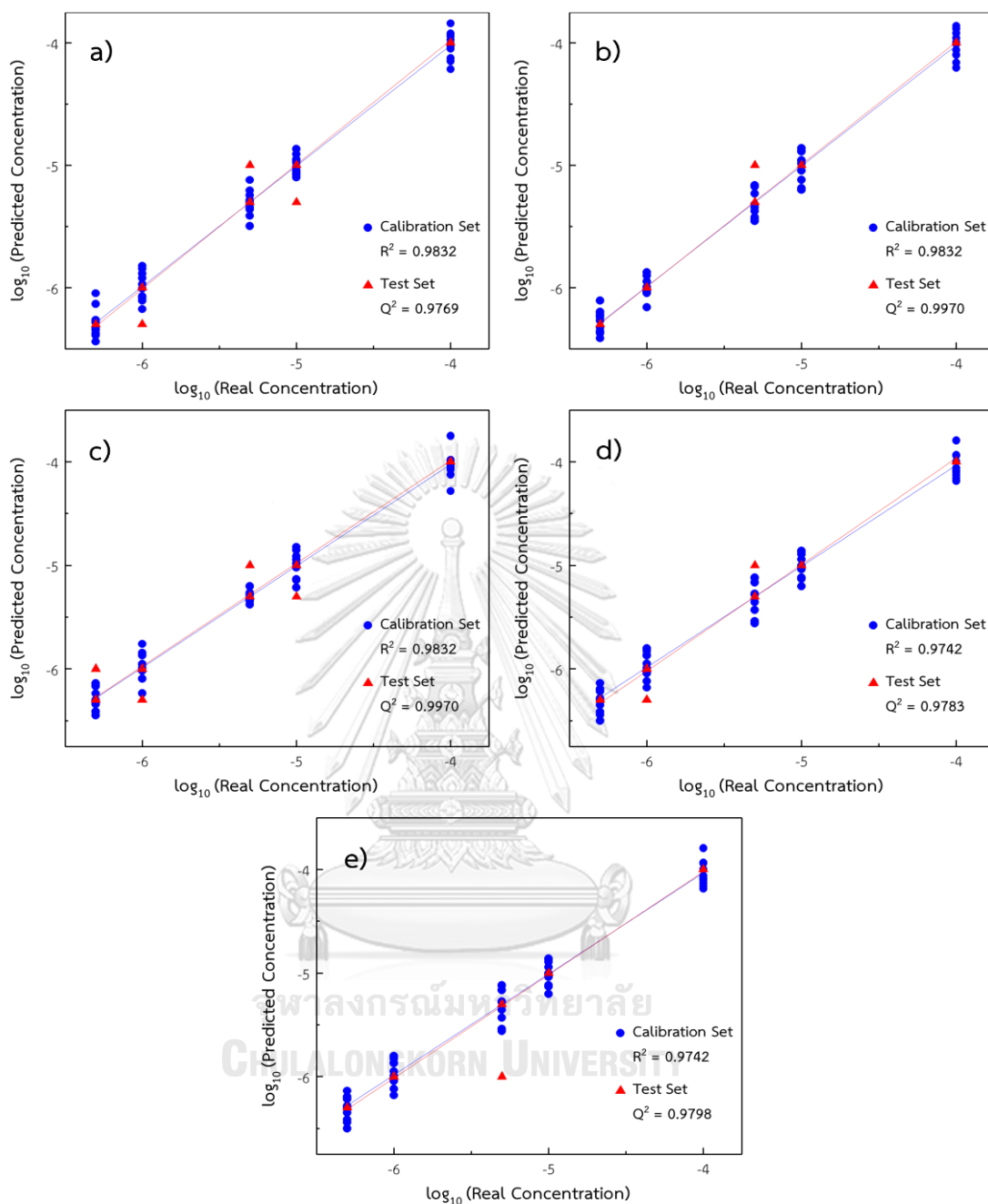


Figure 4.20 PLS models for PhT-modified AgNP films with (a) perylene in the presence of chrysene, (b) perylene in the presence of pyrene, (c) triphenylene in the presence of chrysene, (d) pyrene in the presence of pentacene, and (e) chrysene in the presence of naphthacene.

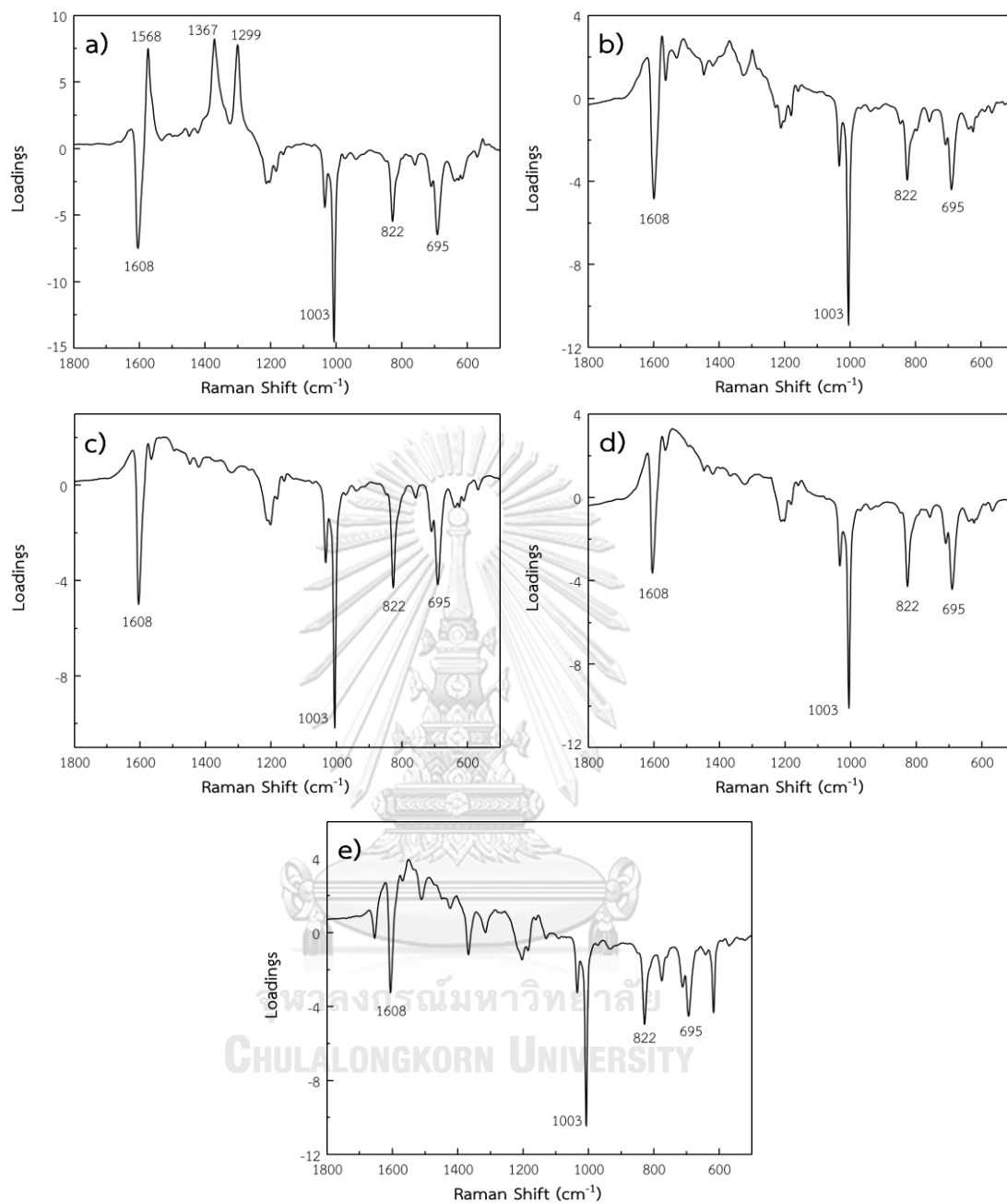


Figure 4.21 First loading plots of PhT-modified AgNP film with (a) perylene in the presence of chrysene, (b) perylene in the presence of pyrene, (c) triphenylene in the presence of chrysene, (d) pyrene in the presence of pentacene, and (e) chrysene in the presence of naphthacene.

From Figure 4.16 and 4.19, some characteristic peaks of PAHs can be observed directly from raw spectra that used NT- and PhT-modified AgNP film as substrate. For NT-modified AgNP films, the intensities of characteristic peaks from substrates are so strong that it is quite difficult to determine the PAH characteristic peak directly from the obtained spectra. Moreover, the intensity of characteristic peaks from PAHs are harder to analyze due to very low concentrations of PAHs. For quantitative analysis, PLS is also used to determine the relationship between concentration and Raman intensity. From Figure 4.17 and 4.20, the obtained calibration curve from PLS model (blue line) is then plotted together with cross-validation curve (red line). R^2 and Q^2 value indicate that the obtained model can be used to predict the mixture concentrations. Summary of R^2 and Q^2 values are shown in Table 4.13.

To determine the peak that affected by the concentration of the mixture of 2 different PAHs, the first loadings obtained from PLS models were plotted. From Figure 4.18 and 4.21, first loading plots that obtained from PLS model indicate that perylene is hardly be interfered by other PAHs. For NT-modified AgNP film, most of peak intensities decrease when PAH concentration increases as it has a strong Raman signal on its own. By having PAH adsorbed on the surface of the substrate, the substrate will be hindered by PAH resulted in the decrease of the Raman signal intensity. For PhT-modified AgNP film, first loading plots show mostly the peak of substrate with a decrease in intensity when the concentration of PAH increases. The interfering PAH affects the first loading plot, which make the plot different from the one plotted from pure PAH spectra. However, the interfering PAH has no effect on the calibration curve.

Table 4.13 R^2 of calibration curve and Q^2 of LOOCV of 2 PAHs mixture

Substrate	Mixture	Analyzed PAH	Interfering PAH	R^2	Q^2
NT-modified AgNP film	1	Perylene	Chrysene	0.9898	0.9805
	2	Perylene	Pyrene	0.9927	0.9821
	3	Triphenylene	Chrysene	0.9897	0.9487
	4	Pyrene	Pentacene	0.9824	0.8929
	5	Chrysene	Naphthacene	0.9925	0.9946
PhT- modified AgNP film	1	Perylene	Chrysene	0.9832	0.9769
	2	Perylene	Pyrene	0.9832	0.9970
	3	Triphenylene	Chrysene	0.9832	0.9970
	4	Pyrene	Pentacene	0.9742	0.9783
	5	Chrysene	Naphthacene	0.9742	0.9798

4.5 Determination of the total concentration of PAHs in the mixture of nine different PAHs

To determine the total concentration of PAHs, 5 mixtures of 9 different PAHs were prepared with the concentrations as shown in Table 3.2, to create more complicated system. From Figure 4.18, the intensities of overall peaks consistently decrease with a decrease in the total concentration of PAHs. The characteristic peaks of PAHs are difficult to determine because of the overlapping between peaks from substrate and from several PAHs.

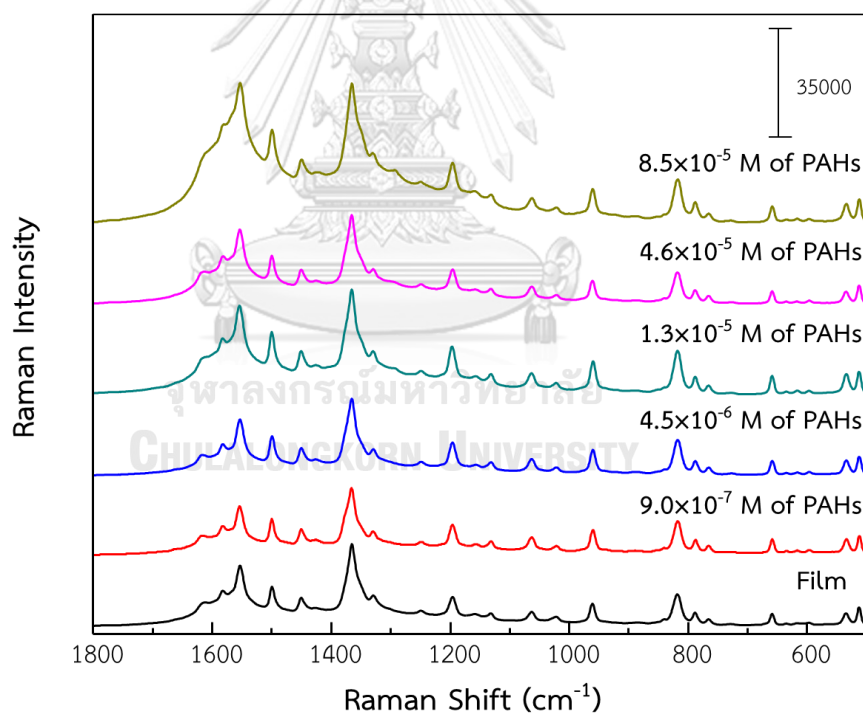


Figure 4.22 SERS spectra of NT-modified AgNP film with the mixtures of 9 different PAHs.

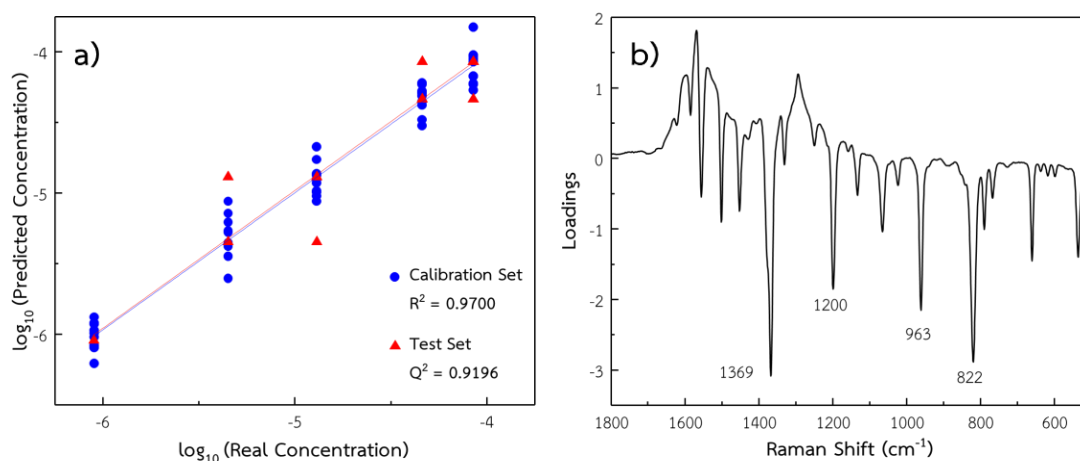


Figure 4.23 (a) PLS model and (b) first loading plot for NT-modified AgNP films with the mixtures of 9 different PAHs.

The calibration curves for the total concentration of 9 different PAHs were created and validated by using PLS and LOOCV, respectively, as shown in Figure 4.20a. From Figure 4.20a, the PLS model obtained from the mixture gives the high R^2 value of 0.9700. The PLS model was then cross validated with LOOCV. The obtained Q^2 of 0.9196 indicates that the PLS model can predict the total concentration of PAHs effectively. From Figure 4.19b, the peaks at 1369, 1200, 963, and 822 cm^{-1} correspond to C–C stretching, in-plane C–H bending, out of plane C–H bending, and ring deformation, respectively. These peaks are the characteristic peaks of substrate that disturbed by the presence of several PAHs. This result suggests that NT-modified AgNP film can accumulate PAHs on the surfaces of AgNPs and enhance Raman signals of these PAHs. Therefore, NT-modified AgNP film can be used to determine the mixtures of 9 different PAHs, which represents a more complex system, given the results of total concentration of PAHs.

CHAPTER 5

CONCLUSIONS

5.1 Conclusions

SERS technique can be used to detect 9 different PAHs. The 5 different thiol-modified AgNP films; PT, OT, NT, PhT, or DT, were fabricated by LB method on glass slide. Thiol compounds are important for fabricating the LB film. They act as a surfactant, induce AgNPs to move to the aqueous/organic interface, and forming AgNP film. The fabricated substrates are used as SERS substrates which can detect PAHs individually and in the mixture of different PAHs. The functionalization plays an important role in creating suitable hot spots for PAHs which are non-polar and cannot be adsorbed on a bare silver surface. The selection of suitable substrate for PAH can be done by the help of PCA and cluster separation. In this work, DBI is selected to use as cluster separation index. The lower value of DBI indicates the better separation of substrate and substrate that has PAH attach on. NT-modified AgNP film is selected for the detection of anthracene, chrysene, naphthacene, naphthalene, and triphenylene while PhT-modified AgNP film is selected for the detection of perylene and pentacene. Phenanthrene and pyrene can be detected effectively with PT-modified AgNP film. For quantitative analysis, the spectra are processed with PLS regression with the R^2 value of calibration curve more than 0.9800. The obtained PLS model is then cross validated using LOOCV technique, the obtained Q^2 value (R^2 value for cross validation) more than 0.8900. This indicates that the obtained calibration curve can predict the concentration of each PAH effectively.

To investigate the sensitivity of substrate, the mixtures of 2 different PAHs are detected. The achieved spectra from mixtures undergo PLS and LOOCV procedure with the given R^2 and Q^2 value more than 0.9800 and 0.9300, respectively. The total concentration of PAHs in the mixtures of 9 different PAHs can be detected and undergo PLS and LOOCV procedure. The achieved PLS and cross-validation model has a R^2 and Q^2 value 0.9700 and 0.9196, respectively, indicating the ability of substrate for the detection of PAHs in the complex system.

From overall results, SERS technique using the fabricated thiol-modified films, which has a simple fabricating procedure, can be used to detect PAH in pure PAH solutions, at the concentration ranging from 10^{-4} – 10^{-7} M, and mixtures of different PAHs. Finally, SERS technique provides an advantage of sample analysis which does not require any sample pretreatment compared to other techniques. It also provides a convenient *in situ* analysis with inexpensive expenses and high sensitivity results.

5.2 Suggestions

The detection of PAHs in the real matrix can be done using the fabricated thiol-modified AgNP films. Because PAHs are non-polar, we suggest using the polar matrix despite non-polar matrix. In non-polar matrix, such as oil, PAHs will prefer to be in the matrix rather than attach on the substrate surface. This will make other components in matrix randomly attach on the substrate and are detected while performing SERS measurement. In polar matrix, such as sea water, PAHs will be forced to migrate from matrix to substrate surface which will expected to be detected effectively with SERS technique.

REFERENCES

1. Bartle, K. D.; Lee, M. L.; Wise, S. A., Modern analytical methods for environmental polycyclic aromatic compounds. *Chemical Society Reviews* **1981**, *10* (1), 113-158.
2. Gilbert, J., The fate of environmental contaminants in the food chain. *Science of The Total Environment* **1994**, *143* (1), 103-111.
3. Alexander, J.; Benford, D.; Cockburn, A.; Cravedi, J.-P.; Dogliotti, E.; Domenico, A. D.; Fernández-Cruz, M. L.; Fink-Gremmels, J.; Fürst, P.; Galli, C.; Grandjean, P.; Gzyl, J.; Heinemeyer, G.; Johansson, N.; Mutti, A.; Schlatter, J.; Leeuwen, R. v.; Peteghem, C. V.; Verger, Philippe, Polycyclic Aromatic Hydrocarbons in Food Scientific Opinion of the Panel on Contaminants in the Food Chain. *The EFSA Journal* **2008**, *724*, 114.
4. Khalili, N. R.; Scheff, P. A.; Holsen, T. M., PAH source fingerprints for coke ovens, diesel and, gasoline engines, highway tunnels, and wood combustion emissions. *Atmospheric Environment* **1995**, *29* (4), 533-542.
5. Budzinski, H.; Jones, I.; Bellocq, J.; Piérard, C.; Garrigues, P., Evaluation of sediment contamination by polycyclic aromatic hydrocarbons in the Gironde estuary. *Marine Chemistry* **1997**, *58* (1), 85-97.
6. Venkataraman, C.; Friedlander, S. K., Size Distributions of Polycyclic Aromatic Hydrocarbons and Elemental Carbon. 2. Ambient Measurements and Effects of

- Atmospheric Processes. *Environmental Science & Technology* **1994**, *28* (4), 563-572.
7. Buseti, F.; Heitz, A.; Cuomo, M.; Badoer, S.; Traverso, P., *Determination of Sixteen Polycyclic Aromatic Hydrocarbons in Aqueous and Solid Samples from an Italian Wastewater Treatment Plant*. 2006; Vol. 1102, p 104-15.
 8. Péron, O.; Rinnert, E.; Lehaitre, M.; Crassous, P.; Compère, C., Detection of polycyclic aromatic hydrocarbon (PAH) compounds in artificial sea-water using surface-enhanced Raman scattering (SERS). *Talanta* **2009**, *79* (2), 199-204.
 9. Leyton, P.; Sanchez-Cortes, S.; Garcia-Ramos, J. V.; Domingo, C.; Campos-Vallette, M.; Saitz, C.; Clavijo, R. E., Selective Molecular Recognition of Polycyclic Aromatic Hydrocarbons (PAHs) on Calix[4]arene-Functionalized Ag Nanoparticles by Surface-Enhanced Raman Scattering. *The Journal of Physical Chemistry B* **2004**, *108* (45), 17484-17490.
 10. Xie, Y.; Wang, X.; Han, X.; Song, W.; Ruan, W.; Liu, J.; Zhao, B.; Ozaki, Y., Selective SERS detection of each polycyclic aromatic hydrocarbon (PAH) in a mixture of five kinds of PAHs. *Journal of Raman Spectroscopy* **2011**, *42* (5), 945-950.
 11. Jiang, M.; Qian, Z.; Zhou, X.; Xin, X.; Wu, J.; Chen, C.; Zhang, G.; Xu, G.; Cheng, Y., CTAB micelles assisted rGO-AgNP hybrids for SERS detection of polycyclic aromatic hydrocarbons. *Physical Chemistry Chemical Physics* **2015**, *17* (33), 21158-21163.

12. Bao, L.; Sheng, P.; Li, J.; Wu, S.; Cai, Q.; Yao, S., Surface enhanced Raman spectroscopic detection of polycyclic aromatic hydrocarbons (PAHs) using a gold nanoparticles-modified alginate gel network. *Analyst* **2012**, *137* (17), 4010-4015.
13. Schmidt, H.; Bich Ha, N.; Pfannkuche, J.; Amann, H.; Kronfeldt, H.-D.; Kowalewska, G., Detection of PAHs in seawater using surface-enhanced Raman scattering (SERS). *Marine Pollution Bulletin* **2004**, *49* (3), 229-234.
14. Lucht, S.; Murphy, T.; Schmidt, H.; Kronfeldt, H. D., Optimized recipe for sol-gel-based SERS substrates. *Journal of Raman Spectroscopy* **2000**, *31* (11), 1017-1022.
15. Agency for Toxic Substances and Disease Registry (ATSDR), Toxicological Profile for Polycyclic Aromatic Hydrocarbons (PAHs). *Atlanta, GA: U.S. Department of Health and Human Services, Public Health Service. 1995.*
16. Agency for Toxic Substances and Disease Registry (ATSDR), ToxFAQs™ for Polycyclic Aromatic Hydrocarbons (PAHs). *Atlanta, GA: U.S. Department of Health and Human Services, Public Health Service. 1996.*
17. Zelinkova, Z.; Wenzl, T., The Occurrence of 16 EPA PAHs in Food – A Review. *Polycyclic Aromatic Compounds* **2015**, *35* (2-4), 248-284.
18. Boström, C.-E.; Gerde, P.; Hanberg, A.; Jernström, B.; Johansson, C.; Kyrklund, T.; Rannug, A.; Törnqvist, M.; Victorin, K.; Westerholm, R., Cancer risk assessment, indicators, and guidelines for polycyclic aromatic hydrocarbons in the ambient

- air. *Environmental Health Perspectives* **2002**, 110 (Suppl 3), 451-488.
19. Boffetta, P.; Jourenkova, N.; Gustavsson, P., *Cancer risk from occupational and environmental exposure to polycyclic aromatic hydrocarbons. Cancer Causes Control* 8:444-472. 1997; Vol. 8, p 444-72.
 20. Boehm, P. D., 15 - Polycyclic Aromatic Hydrocarbons (PAHs) A2 - Morrison, Robert D. In *Environmental Forensics*, Murphy, B. L., Ed. Academic Press: Burlington, 1964; pp 313-337.
 21. Larkin, P., *Infrared and Raman Spectroscopy Principles and Spectral Interpretation*. Elsevier: New York, 2011.
 22. Smith, E.; Dent, G., *Modern Raman Spectroscopy: A Practical Approach*. John Wiley & Sons Ltd: Chichester, UK, 2005.
 23. Abalde-Cela, S.; Aldeanueva-Potel, P.; Mateo-Mateo, C.; Rodríguez-Lorenzo, L.; Alvarez-Puebla, R. A.; Liz-Marzán, L. M., Surface-enhanced Raman scattering biomedical applications of plasmonic colloidal particles. *Journal of The Royal Society Interface* **2010**.
 24. Le Ru, E. C.; Etchegoin, P. G., Chapter 8 - Recent developments. In *Principles of Surface-Enhanced Raman Spectroscopy*, Elsevier: Amsterdam, 2009; pp 415-464.
 25. Petryayeva, E.; Krull, U. J., Localized surface plasmon resonance: Nanostructures, bioassays and biosensing—A review. *Analytica Chimica Acta*

- 2011**, 706 (1), 8-24.
26. Willets, K. A.; Duyne, R. P. V., Localized Surface Plasmon Resonance Spectroscopy and Sensing. *Annual Review of Physical Chemistry* **2007**, 58 (1), 267-297.
 27. Aroca, R., Surface-Enhanced Infrared Spectroscopy. In *Surface-Enhanced Vibrational Spectroscopy*, John Wiley & Sons, Ltd: 2007.
 28. Rivera, V. A. G.; Ferri, F. A.; Jr, E. M., Localized Surface Plasmon Resonances: Noble Metal Nanoparticle Interaction with Rare-Earth Ions. In *Plasmonics - Principles and Applications*, Kim, K. Y., Ed. InTech: Rijeka, 2012; p Ch. 11.
 29. Lee, P. C.; Meisel, D., Adsorption and surface-enhanced Raman of dyes on silver and gold sols. *The Journal of Physical Chemistry* **1982**, 86 (17), 3391-3395.
 30. Pienpinijtham, P.; Han, X. X.; Ekgasit, S.; Ozaki, Y., An ionic surfactant-mediated Langmuir-Blodgett method to construct gold nanoparticle films for surface-enhanced Raman scattering. *Physical Chemistry Chemical Physics* **2012**, 14 (29), 10132-10139.
 31. Roberts, G., *Langmuir-Blodgett Films*. Springer US: 1990.
 32. Bezdek, J. C.; Pal, N. R., Some new indexes of cluster validity. *IEEE Transactions on Systems, Man, and Cybernetics, Part B (Cybernetics)* **1998**, 28 (3), 301-315.
 33. Capitaine, H. L.; Frelicot, C., A Cluster-Validity Index Combining an Overlap Measure and a Separation Measure Based on Fuzzy-Aggregation Operators. *IEEE*

- Transactions on Fuzzy Systems* **2011**, 19 (3), 580-588.
34. Chou, C.-H.; Su, M.-C.; Lai, E., A new cluster validity measure and its application to image compression. *Pattern Analysis and Applications* **2004**, 7 (2), 205-220.
35. Davies, D. L.; Bouldin, D. W., A Cluster Separation Measure. *IEEE Transactions on Pattern Analysis and Machine Intelligence* **1979**, PAMI-1 (2), 224-227.
36. Dixon, S. J.; Heinrich, N.; Holmboe, M.; Schaefer, M. L.; Reed, R. R.; Trevejo, J.; Brereton, R. G., Use of cluster separation indices and the influence of outliers: application of two new separation indices, the modified silhouette index and the overlap coefficient to simulated data and mouse urine metabolomic profiles. *Journal of Chemometrics* **2009**, 23 (1), 19-31.
37. Partial Least Squares Regression. In *Wiley StatsRef: Statistics Reference Online*.
38. Geladi, P.; Kowalski, B. R., Partial least-squares regression: a tutorial. *Analytica Chimica Acta* **1986**, 185, 1-17.
39. Cawley, G. C. In *Leave-One-Out Cross-Validation Based Model Selection Criteria for Weighted LS-SVMs*, The 2006 IEEE International Joint Conference on Neural Network Proceedings, 16-21 July 2006; 2006; pp 1661-1668.
40. Cawley, G. C.; Talbot, N. L. C., Efficient leave-one-out cross-validation of kernel fisher discriminant classifiers. *Pattern Recognition* **2003**, 36 (11), 2585-2592.
41. Wong, T.-T., Performance evaluation of classification algorithms by k-fold and leave-one-out cross validation. *Pattern Recognition* **2015**, 48 (9), 2839-2846.

42. Butler, H. J.; Fogarty, S. W.; Kerns, J. G.; Martin-Hirsch, P. L.; Fullwood, N. J.; Martin, F. L., Gold nanoparticles as a substrate in bio-analytical near-infrared surface-enhanced Raman spectroscopy. *Analyst* **2015**, *140* (9), 3090-3097.
43. Amendola, V.; Bakr, O. M.; Stellacci, F., A Study of the Surface Plasmon Resonance of Silver Nanoparticles by the Discrete Dipole Approximation Method: Effect of Shape, Size, Structure, and Assembly. *Plasmonics* **2010**, *5* (1), 85-97.
44. Panda, S. K.; Chakraborti, S.; Basu, R. N., Size and shape dependences of the colloidal silver nanoparticles on the light sources in photo-mediated citrate reduction technique. *Bulletin of Materials Science* **2018**, *41* (4), 90.
45. Akers, K.; Aroca, R.; Hort, A. M.; Loutfy, R. O., Molecular organization in perylene tetracarboxylic di-imide solid films. *Spectrochimica Acta Part A: Molecular Spectroscopy* **1988**, *44* (11), 1129-1135.
46. Harris, D. C.; Bertolucci, M. D., *Symmetry and spectroscopy : an introduction to vibrational and electronic spectroscopy*. Dover: New York, 1989.
47. Scholz, R.; Kobitski, A. Y.; Kampen, T. U.; Schreiber, M.; Zahn, D. R. T.; Jungnickel, G.; Elstner, M.; Sternberg, M.; Frauenheim, T., Resonant Raman spectroscopy of 3,4,9,10-perylene-tetracarboxylic-dianhydride epitaxial films. *Physical Review B* **2000**, *61* (20), 13659-13669.
48. Jones, C. M.; Asher, S. A., Ultraviolet resonance Raman study of the pyrene S4,

- S3, and S2 excited electronic states. *The Journal of Chemical Physics* **1988**, *89* (5), 2649-2661.
49. Abdi, H.; Williams, L. J., Principal component analysis. *Wiley Interdisciplinary Reviews: Computational Statistics* **2010**, *2* (4), 433-459.
50. Wold, S.; Esbensen, K.; Geladi, P., Principal component analysis. *Chemometrics and Intelligent Laboratory Systems* **1987**, *2* (1), 37-52.





จุฬาลงกรณ์มหาวิทยาลัย
CHULALONGKORN UNIVERSITY

VITA

NAME Sathita Taksadej

DATE OF BIRTH 17 July 1993

PLACE OF BIRTH Bangkok

INSTITUTIONS ATTENDED Triamudomsuksa School
Chulalongkorn University

HOME ADDRESS 83 Soi Sukhumvit50 Sukhumvit rd., Phra Khanong, Klong
Toey, Bangkok 10260



จุฬาลงกรณ์มหาวิทยาลัย
CHULALONGKORN UNIVERSITY